

# V-band photometry of asteroids from ASAS-SN

## Finding asteroids with slow spin <sup>★</sup>

J. Hanuš<sup>1</sup>, O. Pejcha<sup>2</sup>, B. J. Shappee<sup>3</sup>, C. S. Kochanek<sup>4,5</sup>, K. Z. Stanek<sup>4,5</sup>, and T. W.-S. Holoien<sup>6,★★</sup>

<sup>1</sup> Institute of Astronomy, Faculty of Mathematics and Physics, Charles University, V Holešovičkách 2, 18000 Prague, Czech Republic

<sup>2</sup> Institute of Theoretical Physics, Faculty of Mathematics and Physics, Charles University, V Holešovičkách 2, 18000 Prague, Czech Republic

<sup>3</sup> Institute for Astronomy, University of Hawai'i, 2680 Woodlawn Drive, Honolulu, HI 96822, USA

<sup>4</sup> Department of Astronomy, The Ohio State University, 140 West 18th Avenue, Columbus, OH 43210, USA

<sup>5</sup> Center for Cosmology and Astroparticle Physics, The Ohio State University, 191 W. Woodruff Avenue, Columbus, OH 43210, USA

<sup>6</sup> The Observatories of the Carnegie Institution for Science, 813 Santa Barbara St., Pasadena, CA 91101, USA

Received x-x-2021 / Accepted x-x-2021

### ABSTRACT

We present *V*-band photometry of the 20,000 brightest asteroids using data from the All-Sky Automated Survey for Supernovae (ASAS-SN) between 2012 and 2018. We were able to apply the convex inversion method to more than 5,000 asteroids with more than 60 good measurements in order to derive their sidereal rotation periods, spin axis orientations, and shape models. We derive unique spin state and shape solutions for 760 asteroids, including 163 new determinations. This corresponds to a success rate of about 15%, which is significantly higher than the success rate previously achieved using photometry from surveys. We derive the first sidereal rotation periods for additional 69 asteroids. We find good agreement in spin periods and pole orientations for objects with prior solutions. We obtain a statistical sample of asteroid physical properties that is sufficient for the detection of several previously known trends, such as the underrepresentation of slow rotators in current databases, and the anisotropic distribution of spin orientations driven by the nongravitational forces. We also investigate the dependence of spin orientations on the rotation period. Since 2018, ASAS-SN has been observing the sky with higher cadence and a deeper limiting magnitude, which will lead to many more new solutions in just a few years.

**Key words.** Minor planets, asteroids: general – Surveys – Methods: observational – Methods: data analysis

## 1. Introduction

A large number of sky surveys have monitored the sky with various depths, cadences, coverage areas, and scientific goals. Examples include the All-Sky Automated Survey (ASAS; Pojmanski 2002), the Optical Gravitational Lensing Experiment (OGLE; Udalski 2003), the Northern Sky Variability Survey (NSVS; Woźniak et al. 2004), MACHO (Alcock et al. 1997), EROS (Palanque-Delabrouille et al. 1998), the Catalina Sky Survey (CSS, Larson et al. 2003), the Asteroid Terrestrial-impact Last Alert System (ATLAS; Tonry et al. 2018), *Gaia* (Gaia Collaboration et al. 2016), the Zwicky Transient Facility (ZTF; Bellm et al. 2019), *Kepler* (Borucki et al. 2010), *TESS* (Ricker et al. 2015), and PanSTARRS (Chambers et al. 2016). Although several surveys were designed specifically to find asteroids, most of them are not primarily dedicated to the study of Solar System bodies, but could be used to do so with some effort (e.g., Durech et al. 2020; Pál et al. 2020; Szabó et al. 2016; Gaia Collaboration et al. 2018).

Long-term calibrated photometry from modern time-domain surveys both from the ground and from space has been an important tool for the physical characterization of Solar System bodies. For example, the Sloan Digital Sky Survey data revealed

a bimodal distribution of the broadband colors of main-belt asteroids caused by differences between rocky and carbonaceous surface compositions (Ivezic et al. 2001). Time series data from *K2* (Szabó et al. 2016) and *TESS* (Pál et al. 2020) were used to determine rotation periods for a large number of asteroids.

The information content in the light curves is not limited to the rotation periods only. Ďurech et al. (2010) presented a database of asteroid rotation periods, pole orientations, and three-dimensional (3D) convex shapes determined using the photometry inversion technique of Kaasalainen & Torppa (2001) and Kaasalainen et al. (2001). There are currently (as of February 2021) 5,715 shape models for 3,303 asteroids,<sup>1</sup> and the number of solutions is continuously expanding as new data become available. For example, Ďurech & Hanuš (2018) and Ďurech et al. (2020) determined 3D convex shape models and rotation pole orientations for 129 and 1,800 asteroids using Gaia DR2 and ATLAS photometry, respectively.

Understanding the distribution of spin vectors is important for constraining the evolution of asteroid rotational states. Hanuš et al. (2011) and Hanuš et al. (2013a) identified the signatures of the thermal Yarkovsky–O’Keefe–Radzievskii–Paddack effect (YORP, Bottke et al. 2006), which pushes the spin orientation of smaller asteroids to align perpendicularly to their orbital planes. Even better constraints on individual asteroid properties can be obtained by combining shape modeling with infrared photome-

\* Tables A.1-4 are available at the CDS via anonymous ftp to <http://cdsarc.u-strasbg.fr/> or via <http://cdsarc.u-strasbg.fr/viz-bin/qcat?J/A+A/xxx/Axxx>

\*\* NHFP Einstein Fellow

<sup>1</sup> <https://astro.troja.mff.cuni.cz/projects/damit/>

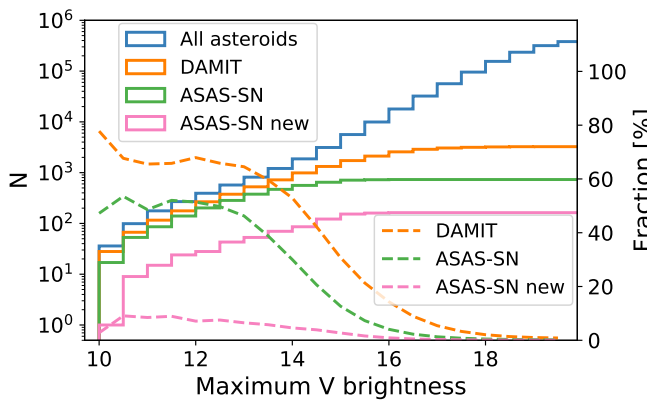


**Fig. 1.** Distributions of asteroids and available shape models as a function of maximum  $V$ -band magnitude. The solid lines show all known asteroids (blue), shape solutions available in the DAMIT database (orange), shape solutions obtained from ASAS-SN data in this work (green), and the asteroids with new shape models from this work (pink). The dashed lines show the percentage of all asteroids that have shape solutions.

try (Hanuš et al. 2015, 2018; Šurech et al. 2017), occultations of stars (Šurech et al. 2011), adaptive optics imaging (Hanuš et al. 2013b, 2017; Viikinkoski et al. 2017, 2018; Vernazza et al. 2018), and interplanetary mission flybys (Preusker et al. 2016a,b, 2017; Watanabe et al. 2019).

Bright asteroids are often the most suitable targets for detailed studies, but the currently available data do not provide a complete picture of the asteroid population. In Figure 1 we show the fraction of asteroids that have shape models as a function of their maximum  $V$ -band magnitude. We see that the completeness is about 70% at the bright end, and begins to decrease for  $V > 14$  mag. More observations, even of bright asteroids, are needed.

In this paper we present  $V$ -band photometry of asteroids obtained with the All-Sky Automated Survey for Supernovae (ASAS-SN, Shappee et al. 2014; Kochanek et al. 2017) between the years 2012 and 2018. During this period ASAS-SN monitored the sky with a cadence of 2–3 days to a depth of  $V \sim 17$  mag using two units in Chile and Hawaii. Although the primary goal of ASAS-SN is the hunt for supernovae (Holoiien et al. 2017) and other transients such as tidal disruption events (Holoiien et al. 2014) or novae (Aydi et al. 2020), it has been used much more broadly to, for example, characterize stellar variability (Jayasinghe et al. 2018, 2019, 2020b; Pawlak et al. 2019; Bredall et al. 2020) or even to discover comets (ASASSN1 or C/2017 O1 and ASASSN2 or C/2018 N2, Prieto et al. 2017; Brinkman 2020; van Buitenen et al. 2018). In this paper we use the calibrated ASAS-SN disk-integrated photometry for the physical characterization of asteroids, in terms of their sidereal rotation periods, spin axis orientation, and 3D shape models.

The structure of our paper is as follows. First, we describe our ASAS-SN data processing pipeline in Sect. 2. Then, we outline the light curve inversion scheme, apply it to ASAS-SN photometry, and derive physical properties for several hundred asteroids in Sect. 3. We discuss our results and derived physical properties in Sect. 4, and conclude our work in Sect. 5.

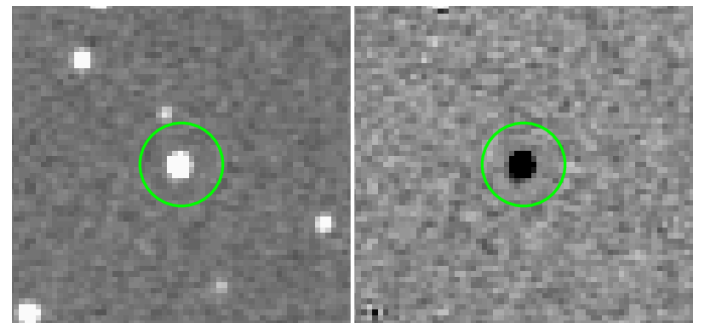


**Fig. 2.** Example of typical images obtained by ASAS-SN. *Left:* Image containing asteroid (130) Elektra with an exposure time of 90 s. *Right:* Corresponding subtracted image (reference image minus observation). The circle of 1 arcmin in radius is centered on the predicted coordinates of Elektra.

## 2. ASAS-SN $V$ -band photometry

During 2012–2018 ASAS-SN consisted of two units in Chile and Hawaii. Each unit consisted of a robotic mount with four 14cm telescopes each with a  $4.5^\circ \times 4.5^\circ$  field of view. The detectors were  $2048^2$  cooled, back-illuminated CCDs with  $8''.0$  pixels, and the image FWHM was roughly 2 pixels. During this period, the survey used a  $V$  filter with a typical limiting magnitude of  $V \sim 17$  mag under good sky conditions. This dataset is the focus of the paper. Since 2018 ASAS-SN has expanded to five units with new mounts in Chile, Texas, and South Africa, and switched to the Sloan  $g$  filter with a limiting magnitude of  $g \sim 18.5$  mag. These observations are continuing and will be the subject of a future work

Each ASAS-SN epoch consists of three (10 pixel) dithered images each with an exposure time of 90 s and roughly 15 s between exposures. The photometry is based on image subtraction followed by aperture photometry on the difference image. In image subtraction a reference image constructed by combining large numbers of high quality images is scaled in flux and PSF structure to match the new data, and is then subtracted to leave an image consisting only of the changes from the reference image (Alard & Lupton 1998; Alard 2000), see an example in Fig. 2. Because the reference image is built from a large number of images, its contribution to the statistical noise is negligible. Fields are observed to optimize the discovery of supernova-like transients based on the age and quality of the last observation. A particular field is visited only once per night. However, there is no fixed temporal spacing (see Fig. 2 in Pawlak et al. 2019), and in searches for variable stars, there is no difficulty with measuring periods of  $\sim 1$  hour (Jayasinghe et al. 2020a,b). Only simple multiples of the diurnal period have significant power in the typical window function.

We performed the absolute calibration using the AAVSO Photometric All-Sky Survey (APASS; Henden et al. 2015) catalog. Ephemeris tables from Miriade accurately predict the location of asteroids in the ASAS-SN data. We selected a region around the predicted position, centered on the emission from the asteroid, and then measured the flux with aperture photometry.

Given the limiting magnitude of  $\sim 17$ , we decided to extract data for the first 10,000 numbered asteroids plus the remaining asteroids predicted to become brighter than  $V = 16.5$  mag. In total, our initial dataset involves  $\sim 20,000$  asteroid light curves. We show the basic statistics in Fig. 3. We have at least 10 flux measurements for  $\sim 19,000$  asteroids, at least 100 for  $\sim 7,000$  as-

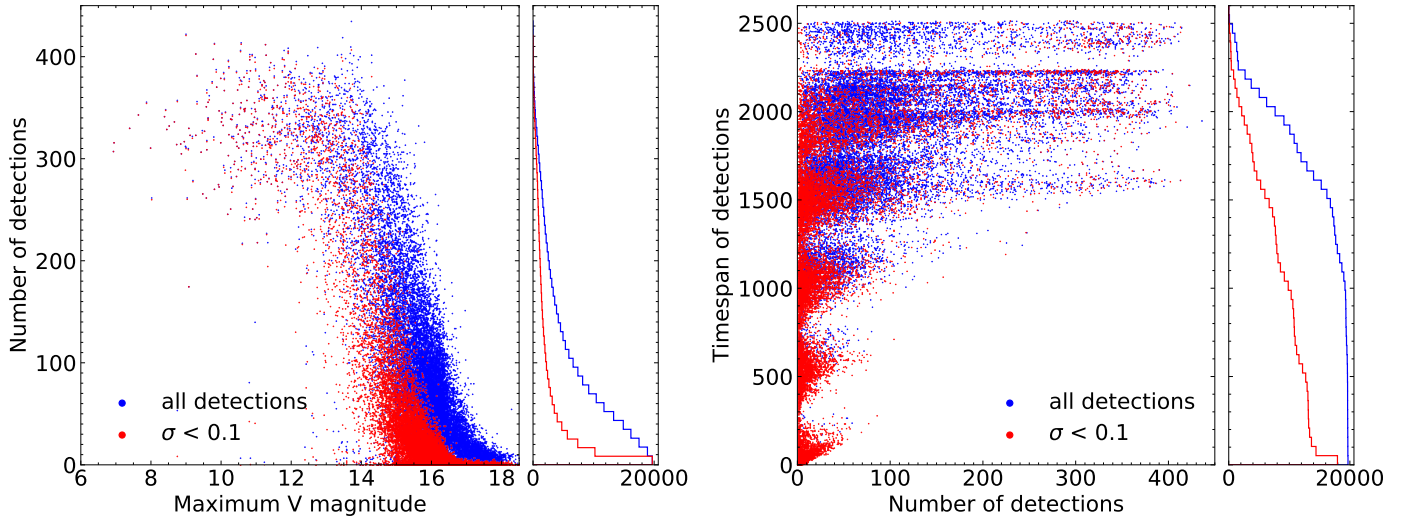


**Fig. 3.** Basic statistics of the ASAS-SN data. *Left:* Number of individual detections for each asteroid as a function of the maximum V-band magnitude predicted by Miriade. *Right:* Timespan of the observations in days as a function of the number of detections. Asteroids with average photometric uncertainties  $\sigma < 0.1$  mag are shown in red.

teroids, and at least 200 for  $\sim 1,000$  asteroids. The average photometric accuracy is  $< 0.1$  mag for about one-third of the objects. About 80% of the asteroids have data spanning more than 1,500 days (4.1 years) corresponding to 3–5 apparitions for each asteroid. Having data from at least three different apparitions (i.e., different viewing geometries) is crucial for successful shape modeling by the light curve inversion technique (Kaasalainen et al. 2001).

Our data contain a significant fraction of clear outliers. To identify them, we use Miriade<sup>2</sup> to obtain the predicted V band magnitude for each epoch. We remove points for which the extracted magnitude differs from the predicted by more than 0.7 magnitude. We selected this threshold because the predicted magnitude reflects the light curve average, while the observed magnitude can correspond to any part of the light curve. Light curve amplitudes (peak to peak) are rarely larger than one magnitude, so our threshold should be sufficiently generous to avoid rejecting real data even for asteroids with extreme amplitudes.

Our data processing follows the standard approach applied to sky survey data (e.g., Hanuš et al. 2011, 2013a; Ďurech et al. 2016; Ďurech & Hanuš 2018; Ďurech et al. 2020). First, we obtain the asterocentric ecliptic coordinates of the Sun and the Earth using Miriade. Having the distances of the asteroid from the Earth, we correct the epochs for light travel times. Then, we transform the magnitudes to intensities, defining a magnitude of 15 to correspond to an intensity of unity for later computational convenience. Next, we normalize the flux intensities to distance of 1 au (astronomical unit) from the Earth and the Sun and average them to unity. We fit the data with a standard phase function (Kaasalainen et al. 2001)

$$f(\alpha) = A_0 \exp \frac{-\alpha}{D} - k\alpha + 1, \quad (1)$$

where  $\alpha$  is the phase angle and  $A_0, D, k$  are free parameters, and then remove any remaining outliers using sigma clipping. We use a clipping threshold of  $2.5\sigma$  based on our empirical experience (also see Ďurech et al. 2020). In cases with a small number of data points ( $\lesssim 30$ ) or a poor sampling of low phase an-

gles ( $\alpha < 10^\circ$ ) the fitting sometimes fails. For these cases we only use the linear part of the phase function for outlier rejection (i.e., we set  $a = 0$ ). As a final step, we keep only measurements with photometric accuracy better than 0.15 mag. This threshold is a reasonable compromise between including too much data with poor photometric quality and removing too many useful measurements. Typical ASAS-SN V-band data are illustrated in Fig. 4 for the main-belt asteroid (130) Elektra.

These steps rejected 30% of the data points on average. The losses were small for bright asteroids (<10% rejected for  $V < 15.5$  mag), but significant for the fainter asteroids (often more than 40–50% for  $V > 16$  mag). Our catalog of ASAS-SN V-band photometry for 19,402 asteroids is presented in Table A.1. For each photometric data point we provide the Julian date, V-band magnitude with the uncertainty, and flags indicating whether the data point was used in the light curve inversion.

For the purpose of the shape modeling by the convex inversion algorithm (Sect. 3), calibrated photometry normalized to unity is sufficient because we only need relative changes of the brightness. The fit of the phase function by a semi-empirical model (Eq. 1) is part of the convex inversion. Therefore, the possible prior conversion to the more common absolute magnitudes  $H_V$  was not needed. Anyone interested in  $H_V$  magnitudes can use our catalog of V-band magnitudes and can do the analysis of the phase function independently.

### 3. Determination of physical parameters by photometry inversion

In this section we describe the light curve inversion scheme we apply to the ASAS-SN V-band data in Sect. 3.1 and the threshold we use to evaluate the uniqueness of the solutions in Sect. 3.2. Finally, we derive new spin state and shape solutions in Sect. 3.3.

#### 3.1. Inversion scheme

We applied the convex inversion (CI) of Kaasalainen & Torppa (2001) and Kaasalainen et al. (2001) to all asteroids with more

<sup>2</sup> <http://vo.imcce.fr/webservices/miriade/>

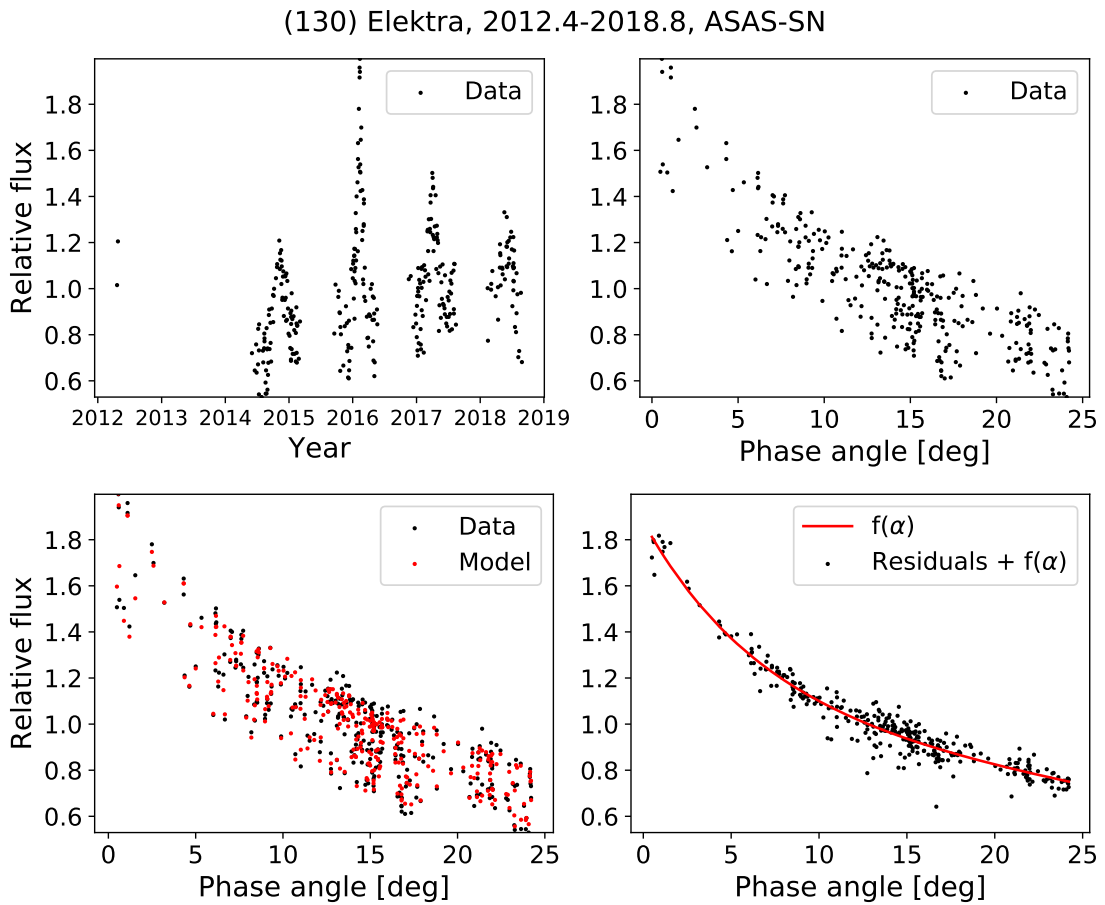


**Fig. 4.** Typical ASAS-SN V-band photometry. *Top row:* ASAS-SN normalized V-band photometry of asteroid (130) Elektra as a function of time (left) and phase angle  $\alpha$  (right). *Bottom row:* Comparison between the observed data and the model for asteroid (130) Elektra as a function of phase angle  $\alpha$  (left) and the fit residuals with respect to the phase function  $f(\alpha)$  (right). The actual  $H_V$  values are not relevant for our study, and therefore the relative flux is used instead.

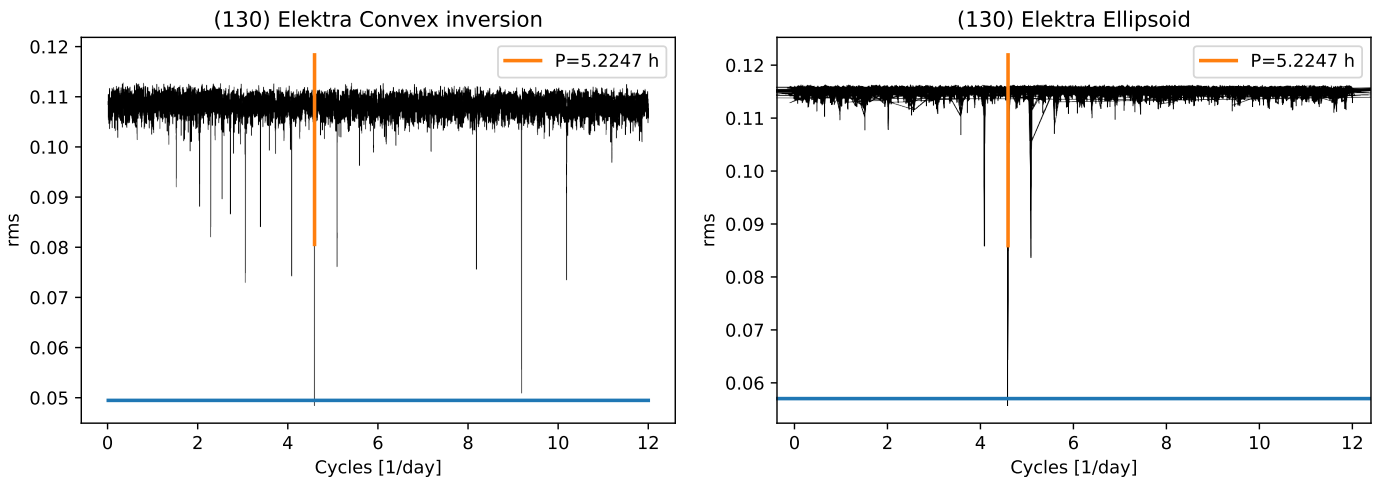


**Fig. 5.** Periodograms (in the frequency domain) of (130) Elektra based on convex inversion (left) and tri-axial ellipsoids (right). Each minimum represents one trial run sampling all the local minima at fixed rotation period. The vertical line indicates the best-fitting value (consistent with the LCDB period of 5.225 h). The horizontal line represents the  $\chi^2$  threshold defined by Eq. 3. There are more than 110,000 trial periods for Elektra (see Eq. 2). The prominent side minima near  $P$  and  $P/2$  are the aliases at  $\pm 0.5$  cycles day $^{-1}$  around  $P$  and  $\pm 1$  cycles day $^{-1}$  around  $P/2$ . Convex inversion models generically show more periodogram structure than the ellipsoidal models.

than 60 individual measurements (5,283 asteroids). This requirement reflects the minimum number of free parameters in the model (55): 49 for shape parameterization, 3 for rotation state (sidereal rotation period, orientation of the spin axis), and 3 phase function parameters (Eq. 1). CI is a gradient-based inversion algorithm that converges to the nearest local minimum given the initial values of the rotation state parameters. We needed to run the minimization multiple times to ensure that we did not miss the global minimum. In practice, the shape modeling consists of four consecutive steps.

In the first step we scan the period interval of 2–1,500 hours. All the asteroids in our sample are large enough to be viewed as rubble piles that cannot rotate faster than the critical rotation period of  $\sim 2$  hours (Pravec & Harris 2000). Rotation periods longer than 1,500 hours are extremely rare and difficult to derive even from sky-survey data. Moreover, these bodies likely rotate in the non-principle axis regime, which we cannot properly model by our method (Pravec et al. 2005). To find the true rotation period, we need to sample a parameter space that is densely filled with local minima. The difference between two local minima in the rotation period parameter space  $\Delta P$  can be approximated as

$$\frac{\Delta P}{P} = \frac{1}{2} \frac{P}{T}, \quad (2)$$

where  $T$  is the time span of the data (Kaasalainen et al. 2001). Therefore, we run the shape models for all periods in the 2–1,500 h interval separated by  $0.5\Delta P$ . For each trial period, we run the shape models with ten different initial pole orientations, isotropically distributed on a sphere.

In the second step, if we find a single rotation period that fits the data significantly better than all the other period values, we run the convex inversion with this period and a finer grid for the initial pole orientations. Our chi-square threshold is defined by

$$\chi_{\text{tr}}^2 = \left(1 + p \sqrt{\frac{2}{v}}\right) \chi_{\min}^2, \quad (3)$$

where  $\chi_{\min}^2$  is the chi-square of the global minimum,  $v$  is the number of degrees of freedom (number of observations minus the number of free parameters), and  $p$  is a weighting factor. We discuss the selection of  $p$  in Sec. 3.2.

In the third step, if we find one or two pole solutions that fit the data better than the remaining ones (again by using Eq. 3), we use the convex inversion algorithm to obtain a unique solution with these poles and rotation period as starting values.

In the fourth step the shape model is represented by a set of areas and their normals (Kaasalainen & Torppa 2001), and the vertices (the shape is represented as a convex polyhedron) are computed using Minkowski minimization (Kaasalainen et al. 1992; Lamberg 1993).

As in Ďurech & Hanuš (2018) and Ďurech et al. (2020), we also use a simple tri-axial ellipsoidal model to scan the rotation period parameter space. These models are easily forced to be physical by requiring the semi-major axes to be  $a > b > c = 1$ . The convention is that  $c$  is the principal rotation axis that maximizes the moment of inertia. While convex inversion often results in similarly good fits for both the correct period  $P$  and its multiples, most commonly  $P/2$ , light curve inversion with tri-axial ellipsoids usually favors only the correct period  $P$  (see Fig. 5). Fortunately, convex inversion solutions with periods  $P/2$  are often nonphysical because they also tend to force the principle rotation axis  $c$  to be the longest, which is nonphysical. We only use the ellipsoidal model for the rotation period and then compute the shape using the convex inversion method.

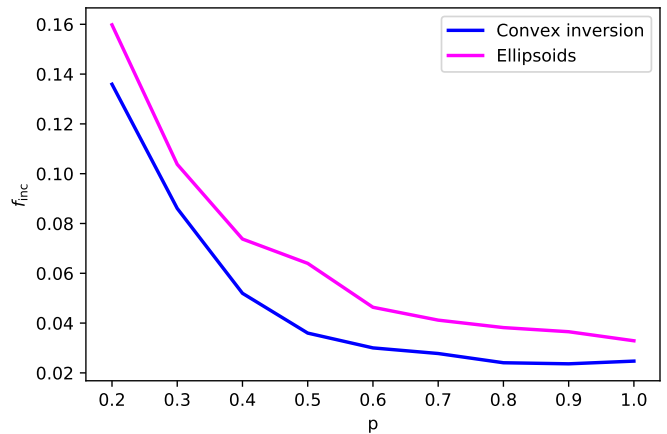


**Fig. 6.** Dependence of the false solution rate  $f_{\text{inc}}$  on the parameter  $p$  defined in Eq. 3 for both the convex inversion (blue) and tri-axial ellipsoid models (magenta).

### 3.2. Period threshold

Our criterion for the uniqueness of the best-fitting rotation period is defined by Eq. 3, where we need to select the optimal value of the  $p$  factor. We do this using comparisons to the asteroid Lightcurve Database (LCDB, Warner et al. 2009) compilation of asteroid physical properties, including rotation periods. Each period is ranked by a flag that indicates its reliability. For our analysis we selected only the most reliable values with flags “3” and “3−”. Figure 6 shows the fraction  $f_{\text{inc}}$  of the ASAS-SN periods that disagree with the previously reported values as a function of  $p$  for the two fitting methods. We omit cases where the LCDB period is twice the ASAS-SN period. For  $p < 0.5$ ,  $f_{\text{inc}}$  increases rather rapidly. So we select  $p = 0.5$  as an optimal value in the CI and  $p = 0.6$  in the tri-axial ellipsoid shape analyses.

For these choices, about 3% of periods derived by CI from ASAS-SN data are inconsistent with the LCDB periods. We discuss several individual cases in Sect. 3.3. It is important to keep in mind that not all flag 3 and 3- periods in LCDB will be correct. Ďurech et al. (2016) and Ďurech et al. (2020) found multiple examples of incorrect estimates and  $f_{\text{inc}}$  on the order of a few percent is not particularly concerning. The incorrect periods were generally for asteroids with  $P > 20$  h, where determinations are more challenging for classical short duration, dense sampling light curve observations. The  $f_{\text{inc}}$  ratio for the tri-axial ellipsoid approach is higher by about 2% than for the convex inversion approach. The minor increase is likely due to the ellipsoidal approach being less physically realistic.

We also see cases where the ASAS-SN period is clearly incorrect. For example, a few tens of the brightest asteroids have at least partly saturated photometry, which sometimes result in best-fitting period values of 24 or 48 h. We rejected these objects from our analysis. Additionally, we also identified cases with a relatively low number of detections ( $< 100$ ) and “suspicious” periodograms. Usually, good periodograms are qualitatively similar to the one of asteroid (130) Elektra (Fig. 5); most of these solutions cluster along the line of constant maximum rms and only several deep and sharp minima are present, usually in simple ratios. Suspicious periodograms have larger scatter and a more random distribution of minima. We also removed these solutions from our analysis. Finally, many solutions with incon-

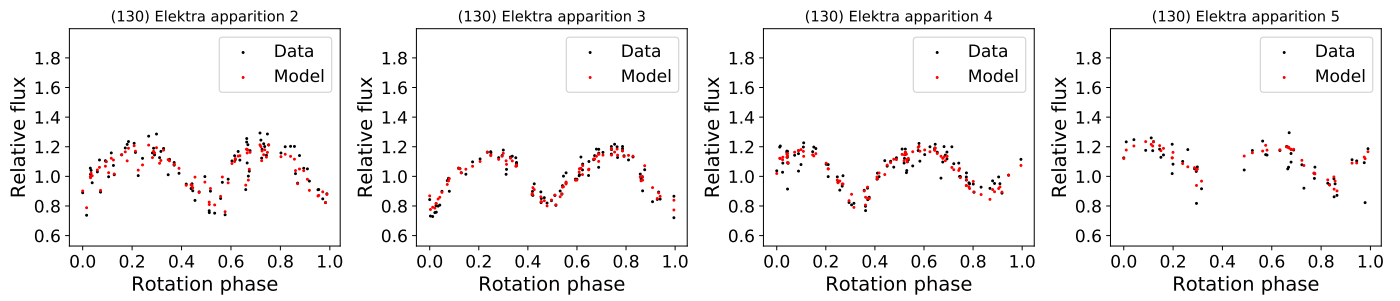


**Fig. 7.** Fit to the ASAS-SN data for asteroid (130) Elektra. The data is split into four apparitions and is shown as a function of rotation phase given the sidereal rotation period of 5.22466 h. The model for each apparition shows scatter because the geometry is also changing during each apparition. The phase reference time is defined independently for each apparition.

sistent LCDB periods were rejected by our additional reliability tests.

We only accepted a solution if it had at most two pole solutions passing the statistical threshold of Eq. 3, and if the two poles were the so called mirror solutions (similar ecliptic latitude and an ecliptic longitude difference of  $\sim 180$  degrees, Kaasalainen & Lamberg 2006). The shape solution also needed to be physically plausible, with the body rotating along its shortest axis. Therefore, we computed the axis with the maximum momentum of inertia of the body (Dobrovolskis 1996) and compared it with the position of the spin axis.

We evaluated the models using the dependence of the brightness on phase angle (Fig. 4) and rotation phase (Fig. 7), which we illustrate using asteroid (130) Elektra. In both cases the mean brightness is normalized to unity. Because the geometry changes with apparition, the phase-folded light curves change with each apparition. The models for each apparition also show scatter due to changes in geometry during the individual apparitions. Similarly, the scatter in the data is a combination of the photometric errors and the changes in geometry. Moreover, the folded plots also illustrate the sufficient coverage of the rotation phase by the data and that the residuals are significantly smaller than the lightcurve amplitude.

### 3.3. New shape solutions from ASAS-SN data

From the 5,283 asteroids with more than 60 photometric measurements, we derived unique spin state and shape solutions for 760 asteroids. This corresponds to a success rate of about 15%, which is significantly higher than the success rate from the previous wide-area surveys such as ATLAS ( $\sim 3\%$ , Ďurech et al. 2020), Gaia DR2 ( $\sim 3\%$ , Ďurech & Hanuš 2018), and Lowell alone or in combination with WISE ( $\lesssim 1\%$ , Ďurech et al. 2016, 2018).

We obtained new shape model determinations for 163 individual asteroids. A typical example is shown in Fig. 9 (asteroid 1532 Inari). We list their physical properties in Table A.2. The solutions for asteroids with shape models already included in DAMIT are provided in Table A.3. Figure 8 compares our pole directions and those reported in DAMIT. The difference is rarely larger than  $30^\circ$ , which suggests a good consistency between our solutions and previous estimates. Additionally, we derived sidereal rotation periods for 69 asteroids for the first time (Table A.4). However, pole orientations for these asteroids remained ambiguous. Clearly, more photometric data are still needed here. Interestingly, the fraction of slowly rotating asteroids is large for these 69 asteroids.

We identified four solutions that were inconsistent with those from DAMIT. Usually, the previous shape modeling was performed over a short interval spanning the rotation period reported in the LCDB database. However, in some cases, either this rotation period was shown to be incorrect or we now prefer a different one (asteroids 1040 and 2962). In two cases, we derived a rotation period that is twice that of DAMIT (asteroids 1461 and 16009).

Within our new shape and spin state solutions, 23 periods are inconsistent with the LCDB periods by more than 5%. Only one has the highest LCDB reliability flag of 3 (asteroid 974). With only one exception (asteroid 1447 Utra), the new periods are larger and typically  $> 100$  h. It is not surprising that these cases generally have lower reliability flags and long periods.

In Figure 10 we show the distribution of rotation periods obtained from ASAS-SN compared to all those available from LCDB. ASAS-SN data are very efficient in identifying long-period rotators due to the long time span and high cadence of the survey. We discuss this issue in Sect. 4.1. Figure 10 also shows the distribution of pole ecliptic longitudes  $\lambda$  and orbital latitudes  $\beta_{\text{orb}}$  for different asteroid sizes, revealing the signatures of YORP in small asteroids. We give more details about this finding in Sect. 4.2. Finally, in Figure 11, we show the distribution of  $\beta_{\text{orb}}$  as a function of rotational period. We discuss the implications of our findings for slow rotators in Sect. 4.3.

## 4. Discussion

ASAS-SN data represent the first sky survey with a fraction of successful shape determinations (15%) exceeding ten percent. This is an order of magnitude improvement over previous efforts based on sparse-in-time datasets. This is partly because of the better photometric accuracy, but also because we limited our analysis to epochs with photometric errors  $< 0.15$  mag. The other analyses typically examined a large number of asteroids close to the detection limit. Such data have photometric uncertainties exceeding 0.15 mag. Moreover, information about the uncertainties is often missing, which precludes filtering based on measurement uncertainty. Shape modeling performed on noisy data usually does not provide a unique solution, which decreases the success rate.

We also tested shape modeling with the photometric uncertainty threshold reduced to 0.1 mag. As expected, the resulting dataset contains fewer asteroids and fewer measurements. However, the brighter asteroids are almost unaffected as their measurements usually have accuracy better than 0.1 mag. The faint asteroids are more affected; the photometric accuracy is

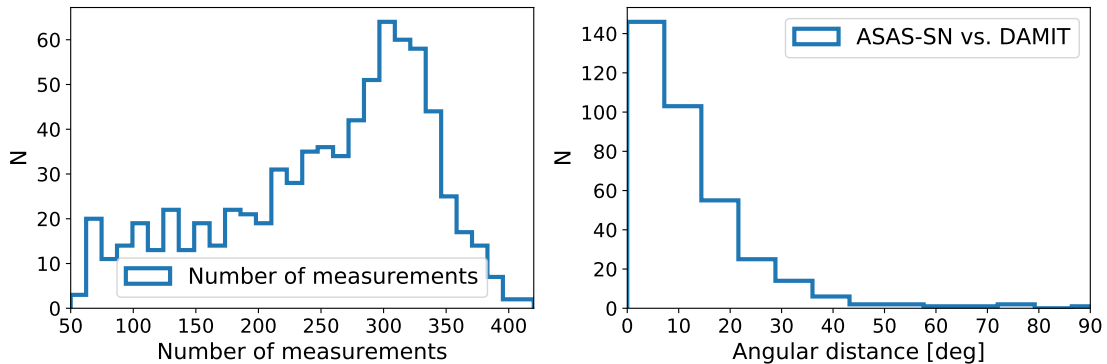


**Fig. 8.** Data amount and pole consistency for ASAS-SN solutions. *Left:* Histogram of the number of ASAS-SN V-band measurements for the asteroids with successful shape solutions. *Right:* Angular distance between the ASAS-SN and DAMIT pole solutions.

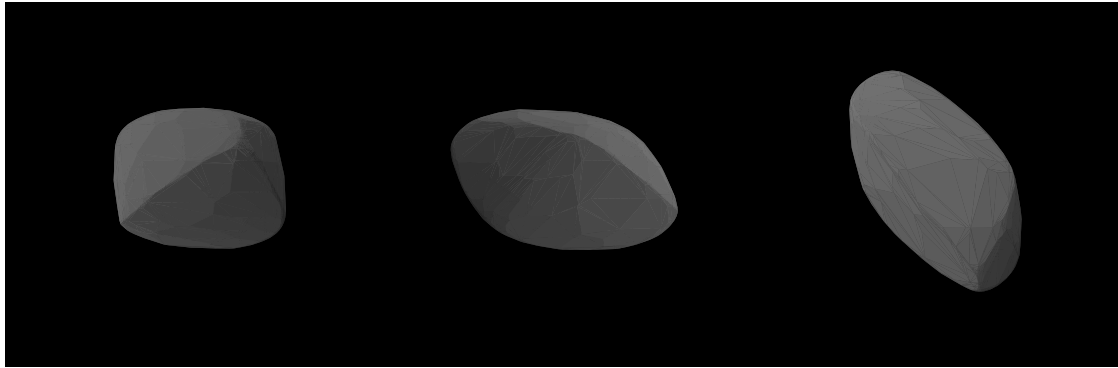


**Fig. 9.** First convex shape model of asteroid (1532) Inari. The left and center views are equatorial with a 90° rotation, while the right view is pole-on.

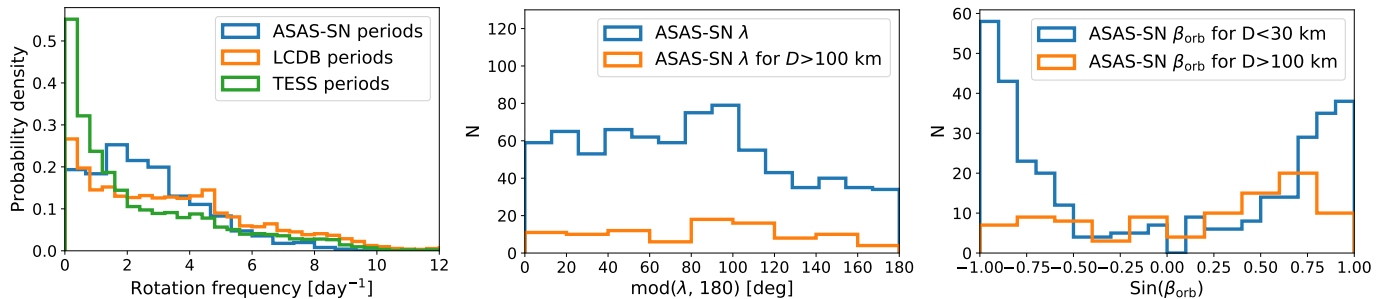


**Fig. 10.** Rotation period and pole direction distributions. *Left:* Normalized period distributions for the ASAS-SN models (760), TESS periods (9,912, Pál et al. 2020), and LCDB periods (31,280, Warner et al. 2009). *Middle:* Distribution of pole ecliptic longitudes  $\lambda$  for all asteroids and asteroids  $> 100$  km derived from the ASAS-SN data. *Right:* Distribution of orbital pole latitudes  $\beta_{\text{orb}}$  derived from ASAS-SN data for asteroids smaller than 30 km and for asteroids larger than 100 km.

often in the 0.1–0.15 mag range. Considering the shape modeling results, the two datasets are rather comparable. In general, adding noisier photometry (i.e., using a threshold of 0.15 mag instead of 0.1 mag) resulted in a small number of missed solutions due to the poorer photometric accuracy, but also produced some additional solutions due to the larger number of measurements available for fainter asteroids. We prefer deriving new solutions for fainter asteroids (i.e., threshold of 0.15 mag) rather than confirming more solutions that are already known.

#### 4.1. Excess of slow rotators

Pál et al. (2020) derived 9,912 rotation periods using TESS data and found a clear excess of slow ( $P \gtrsim 12$  h) rotators compared to existing compilations (their Fig. 7), which suggests these objects were underrepresented in previous ground-based surveys. Similar excesses were also found by Kiss et al. (2019) and Ďurech et al. (2020). This is due to the difficulty of determining long periods using the traditional ground-based observations on which most of the LCDB periods relied (Marciniak et al. 2015, 2018).

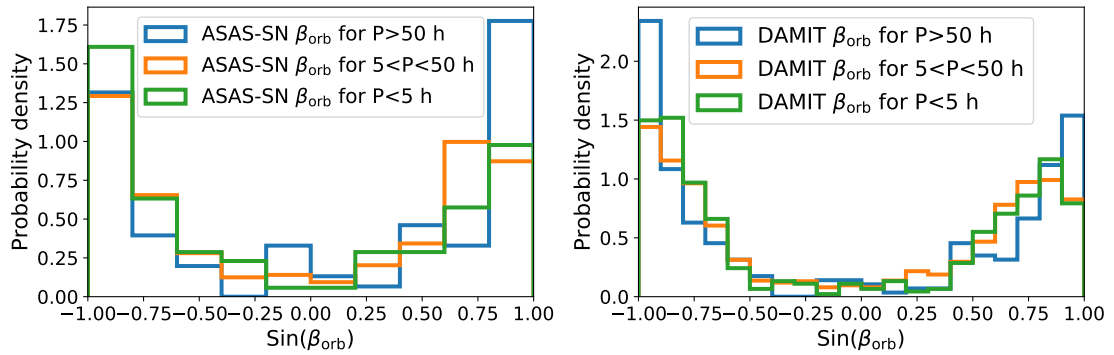


**Fig. 11.** Distribution of orbital pole latitudes  $\beta_{\text{orb}}$  of asteroids with  $D < 50 \text{ km}$  for different rotation period ranges derived from ASAS-SN data (left) and from the DAMIT database (right).

Our sample of 920 ASAS-SN periods show an excess of asteroids with periods between  $\sim 7$  and  $24 \text{ h}$  (see Fig. 10) when compared to the *TESS* (Pál et al. 2020) and the LCDB period distributions. We used the most recent version of the LCDB database with 31,280 period estimates, including all the 9,912 *TESS* periods from Pál et al. (2020). Clearly, periods  $> 24 \text{ h}$  are not as frequent as in the pure *TESS* sample. This likely originates in the smaller success rate of shape model determinations for asteroids with these longer periods because the geometry coverage is probably not sufficient. ASAS-SN data seem to be quite useful for deriving shape models and spin states for asteroids with rotation periods of  $7\text{--}25 \text{ h}$ .

We recall that all the currently available rotation period samples are affected by complicated (often unknown or poorly understood) biases. Therefore, these biases should require proper consideration before any more conclusive interpretations are drawn.

#### 4.2. Spin axis anisotropy

The clustering of spin vectors for asteroids smaller than  $\sim 30 \text{ km}$  was already illustrated and explained by Hanuš et al. (2011), and further confirmed in larger datasets (Hanuš et al. 2013a; Ďurech et al. 2016). The thermal forces known as the YORP effect (Bottke et al. 2006; Vokrouhlický et al. 2003) drive a gradual evolution of the spin axis to be perpendicular to the orbital plane. The pole latitudes of the spin axis should cluster near  $|\sin\beta_{\text{orb}}| = 1$  in our notation. We note that CI provides the pole orientation in the ecliptic coordinate frame  $(\lambda, \beta)$  and we need to transform it into the orbital frame of the asteroid, where the obliquity of the pole is  $\epsilon = 90^\circ - \beta_{\text{orb}}$ . As the orbital inclinations of typical main-belt asteroids are small ( $\lesssim 20^\circ$ ), the differences between  $\beta$  and  $\beta_{\text{orb}}$  are rather small as well.

We clearly see the latitude clustering in our data for asteroids smaller than  $30 \text{ km}$  (Fig. 10), where the YORP timescale is shorter than the reorientation timescale due to collisions (Hanuš et al. 2011). Large asteroids ( $D > 100 \text{ km}$ ) are not significantly affected by the YORP effect and their pole latitudes are randomly distributed (Fig. 10), as expected for a collisionally dominated population. However, there is a statistically significant excess of prograde rotators ( $\beta_{\text{orb}} > 0^\circ$ ) that can be explained by accretion of the pebbles into protoplanets in the prograde-rotating gaseous disk (Johansen & Lacerda 2010).

Bowell et al. (2014) noted that their distribution of ecliptic longitudes was anisotropic. We see a similar distribution of ecliptic longitudes (Fig. 10) with an excess of asteroids at lon-

gitudes of  $60\text{--}110^\circ$ . The anisotropy also seems to be present for large asteroids ( $> 100 \text{ km}$ , Fig. 10), which suggests it is independent of the size. Interestingly, our latitude distribution for asteroids larger than  $100 \text{ km}$  is based on 96 solutions, almost half of the whole population (about 200 bodies). The anisotropic distribution of the ecliptic longitudes remains unexplained.

The observed longitude and latitude distributions are affected by observing biases. Hanuš et al. (2011) performed debiasing of these distributions and showed that the debiased latitude distribution for small asteroids is still clearly anisotropic. Moreover, the observation bias in the longitude is negligible, and thus cannot explain the observed anisotropy.

#### 4.3. Spin states of slow rotators

Asteroids having  $P > 50 \text{ h}$  make up a peculiar group, and are not yet fully understood. There are only about 300 such systems in DAMIT and here we have added an additional 45. The general consensus is that these bodies were de-accelerated by the YORP thermal effect (e.g., Čapek & Vokrouhlický 2004; Pravec et al. 2008). This is in agreement with the population being composed only of small asteroids ( $D < 50 \text{ km}$ ). Larger asteroids have a Maxwellian distribution of rotation periods consistent with their collisional origin (Pravec et al. 2008). However, alternative theories have also been put forward. For instance, some fragments of disruptive collisions could have slow spin rates or the slow rotation could originate in a synchronous binary that split apart. Moreover, a large fraction of slow rotators are in an excited rotation state, the so-called tumbling mode (Harris & Young 1980; Pravec et al. 2005, 2008). There are two main scenarios proposed for the excitation: YORP spin-up eventually self-triggering the tumbling (Vokrouhlický et al. 2007) or YORP spin-up followed by a noncatastrophic collision (Henych & Pravec 2013).

In Fig. 11 we show the pole latitude  $\beta_{\text{orb}}$  distributions for three different bins in rotation period, including slow rotators ( $P > 50 \text{ h}$ ), for the ASAS-SN solutions and for those in DAMIT. For both datasets the slow rotators have a larger number of poles near  $\beta_{\text{orb}} = \pm 90^\circ$  compared to the rest of the population, so there are more spin vectors in the YORP end states. The natural explanation would be that the population of slow rotators is more strongly affected by YORP. It takes more time to slow the period to  $P > 50 \text{ h}$ , and so there is enough time to reach the YORP spin vector end state. A minor complication to this scenario is the presence of secular spin-orbit resonances in which the spin vectors could be temporarily trapped, as in the case of the Koronis family (Slivan 2002; Vokrouhlický et al. 2003).

These resonances are likely responsible for the asymmetry in the  $\beta_{\text{orb}}$  distribution for asteroids with  $D < 30$  km because they affect only the prograde-rotating asteroids. However, as the excess of spin vectors in the end states of slow rotators is present for both prograde and retrograde bodies, the resonances cannot be the main cause. Another process that acts against the YORP evolution is noncatastrophic collisions. As the slow rotators have a rather small moment of inertia compared to the faster rotators, even a small collision can significantly affect the rotation state. For instance, an impact can change the orientation of the spin axis, the value of rotation period (in both directions) or even excite the rotation. More spin state data combined with dynamical studies should shed more light into the processes that are the most active in shaping the population of slow rotators.

## 5. Conclusion

We showed that ASAS-SN V band photometry is a good tool for the physical characterization of asteroids by deriving shapes and rotation properties for 760 asteroids, including 163 new determinations. We validated our results by comparison with determinations based on independent photometric datasets. We also revised incorrect period estimates for several asteroids.

We obtained a statistical sample of asteroid physical properties that was sufficient to confirm and expand on several previously known trends: (i) the underrepresentation of slow rotators in current databases of rotation period estimates (i.e., LCDB) due to observation biases, (ii) the anisotropic distribution of ecliptic pole-latitudes due to nongravitational forces (YORP), and (iii) an anisotropic distribution of ecliptic pole-longitudes of unknown origin.

Most of the successful solutions are for asteroids with more than 200 measurements (Fig. 8), which means that the data cover at least 1,500 days (Fig. 3). Clearly, a good coverage of observing geometries is essential for a successful shape model determination. The asteroid also has to be bright enough during the apparition when it has the faintest apparent V-band magnitude (the least convenient geometry, when the asteroid is at aphelion). Asteroids that are too faint at this apparition are likely too faint or have very noisy photometry at the other apparitions.

The newer ASAS-SN *g*-band data will be quite useful for the shape modeling as they are about one magnitude deeper. Apparitions with poor photometric accuracy or brightness at or slightly below our 16.5 mag threshold in this paper will have useful *g*-band measurements, which could increase the number of successful solutions by a factor of at least 2, particularly since the number of asteroids rises from  $\sim 20,000$  that reach  $V \leq 16.5$  mag to  $\sim 55,000$  that reach  $V \leq 17.5$  mag. Another benefit of the *g*-band data is that one-day aliasing will likely be minimized because ASAS-SN now has units at four different longitudes (at least two for everywhere on the sky). Finally, the full potential of ASAS-SN data lies in the possibility of combination with other datasets, as has been done with others surveys in DAMIT.

**Acknowledgements.** We thank the Las Cumbres Observatory and its staff for its continuing support of the ASAS-SN project. ASAS-SN is supported by the Gordon and Betty Moore Foundation through grant GBMF5490 to the Ohio State University, and NSF grants AST-1515927 and AST-1908570. Development of ASAS-SN has been supported by NSF grant AST-0908816, the Mt. Cuba Astronomical Foundation, the Center for Cosmology and AstroParticle Physics at the Ohio State University, the Chinese Academy of Sciences South America Center for Astronomy (CAS-SACA), the Villum Foundation, and George Skestos.

The work of JH and OP has been supported by INTER-EXCELLENCE grant LTAUSA18093 from the Ministry of Education, Youth, and Sports. The

research of JH has been additionally supported by the Czech Science Foundation through grant 20-08218S and by Charles University Research program No. UNCE/SCI/023. The research of OP has been supported also by Horizon 2020 ERC Starting Grant ‘Cat-In-hAT’ (grant agreement no. 803158). BJS, CSK, and KZS are supported by NSF grant AST-1907570. BJS is also supported by NASA grant 80NSSC19K1717 and NSF grants AST-1920392 and AST-1911074. CSK and KZS are supported by NSF grant AST-181440.

Support for TW-SH was provided by NASA through the NASA Hubble Fellowship grant HST-HF2-51458.001-A awarded by the Space Telescope Science Institute, which is operated by the Association of Universities for Research in Astronomy, Inc., for NASA, under contract NASS-26555.

This research has made use of the Minor Planet Physical Properties Catalogue (MP3C) of the Observatoire de la Côte d’Azur and the IMCCE’s Miriade VO tool.

## References

- Alard, C. 2000, A&AS, 144, 363
- Alard, C. & Lupton, R. H. 1998, ApJ, 503, 325
- Alcock, C., Allsman, R. A., Alves, D., et al. 1997, ApJ, 486, 697
- Aydi, E., Sokolovsky, K. V., Chomaliuk, L., et al. 2020, Nature Astronomy, 4, 776
- Bellm, E. C., Kulkarni, S. R., Graham, M. J., et al. 2019, PASP, 131, 018002
- Borucki, W. J., Koch, D., Basri, G., et al. 2010, Science, 327, 977
- Bottke, J. W. F., Vokrouhlický, D., Rubincam, D. P., & Nesvorný, D. 2006, Annual Review of Earth and Planetary Sciences, 34, 157
- Bowell, E., Oszkiewicz, D. A., Wasserman, L. H., et al. 2014, Meteoritics and Planetary Science, 49, 95
- Bredall, J. W., Shappee, B. J., Gaidos, E., et al. 2020, MNRAS, 496, 3257
- Brinkman, C. L. 2020, in American Astronomical Society Meeting Abstracts, Vol. 235, American Astronomical Society Meeting Abstracts #235, 454.02
- Čapek, D. & Vokrouhlický, D. 2004, Icarus, 172, 526
- Chambers, K. C., Magnier, E. A., Metcalfe, N., et al. 2016, arXiv e-prints, arXiv:1612.05560
- Dobrovolskis, A. R. 1996, Icarus, 124, 698
- Ďurech, J., Delbo', M., Carry, B., Hanuš, J., & Alí-Lagoa, V. 2017, A&A, 604, A27
- Ďurech, J., Hanuš, J., Oszkiewicz, D., & Vančo, R. 2016, A&A, 587, A48
- Ďurech, J. & Hanuš, J. 2018, A&A, 620, A91
- Ďurech, J., Hanuš, J., & Alí-Lagoa, V. 2018, A&A, 617, A57
- Ďurech, J., Kaasalainen, M., Herald, D., et al. 2011, Icarus, 214, 652
- Ďurech, J., Sidorin, V., & Kaasalainen, M. 2010, A&A, 513, A46
- Gaia Collaboration, Prusti, T., de Bruijne, J. H. J., et al. 2016, A&A, 595, A1
- Gaia Collaboration, Spoto, F., Tanga, P., et al. 2018, A&A, 616, A13
- Hanuš, J., Delbo', M., Ďurech, J., & Alí-Lagoa, V. 2015, Icarus, 256, 101
- Hanuš, J., Delbo', M., Ďurech, J., & Alí-Lagoa, V. 2018, Icarus, 309, 297
- Hanuš, J., Ďurech, J., Brož, M., et al. 2013a, A&A, 551, A67
- Hanuš, J., Ďurech, J., Brož, M., et al. 2011, A&A, 530, A134
- Hanuš, J., Marchis, F., & Ďurech, J. 2013b, Icarus, 226, 1045
- Hanuš, J., Viikinkoski, M., Marchis, F., et al. 2017, A&A, 601, A114
- Harris, A. W. & Young, J. W. 1980, Icarus, 43, 20
- Henden, A. A., Levine, S., Terrell, D., & Welch, D. L. 2015, in American Astronomical Society Meeting Abstracts, Vol. 225, American Astronomical Society Meeting Abstracts #225, 336.16
- Henych, T. & Pravec, P. 2013, MNRAS, 432, 1623
- Holoien, T. W. S., Prieto, J. L., Bersier, D., et al. 2014, MNRAS, 445, 3263
- Holoien, T. W. S., Stanek, K. Z., Kochanek, C. S., et al. 2017, MNRAS, 464, 2672
- Ivezić, Ž., Tabachnik, S., Rafikov, R., et al. 2001, AJ, 122, 2749
- Jayasinghe, T., Kochanek, C. S., Stanek, K. Z., et al. 2018, MNRAS, 477, 3145
- Jayasinghe, T., Stanek, K. Z., Kochanek, C. S., et al. 2019, MNRAS, 486, 1907
- Jayasinghe, T., Stanek, K. Z., Kochanek, C. S., et al. 2020a, MNRAS, 491, 13
- Jayasinghe, T., Stanek, K. Z., Kochanek, C. S., et al. 2020b, MNRAS, 493, 4186
- Johansen, A. & Lacerda, P. 2010, MNRAS, 404, 475
- Kaasalainen, M. & Lamberg, L. 2006, Inverse Problems, 22, 749
- Kaasalainen, M., Lamberg, L., Lumme, K., & Bowell, E. 1992, A&A, 259, 318
- Kaasalainen, M. & Torppa, J. 2001, Icarus, 153, 24
- Kaasalainen, M., Torppa, J., & Muinonen, K. 2001, Icarus, 153, 37
- Kiss, C., Szakáts, R., Molnár, L., et al. 2019, in EPSC-DPS Joint Meeting 2019, Vol. 2019, EPSC-DPS2019-848
- Kochanek, C. S., Shappee, B. J., Stanek, K. Z., et al. 2017, PASP, 129, 104502
- Lamberg, L. 1993, PhD thesis, University of Helsinki
- Larson, S., Beshore, E., Hill, R., et al. 2003, in Bulletin of the American Astronomical Society, Vol. 35, AAS/Division for Planetary Sciences Meeting Abstracts #35, 982
- Marciniak, A., Bartczak, P., Müller, T., et al. 2018, A&A, 610, A7
- Marciniak, A., Pilcher, F., Oszkiewicz, D., et al. 2015, Planet. Space Sci., 118, 256

- Pál, A., Szakáts, R., Kiss, C., et al. 2020, *ApJS*, 247, 26  
 Palanque-Delabrouille, N., Afonso, C., Albert, J. N., et al. 1998, *A&A*, 332, 1  
 Pawlak, M., Pejcha, O., Jakubčík, P., et al. 2019, *MNRAS*, 487, 5932  
 Pojmanski, G. 2002, *Acta Astron.*, 52, 397  
 Pravec, P. & Harris, A. W. 2000, *Icarus*, 148, 12  
 Pravec, P., Harris, A. W., Scheirich, P., et al. 2005, *Icarus*, 173, 108  
 Pravec, P., Harris, A. W., Vokrouhlický, D., et al. 2008, *Icarus*, 197, 497  
 Preusker, F., Scholten, F., Matz, K. D., et al. 2016a, in *Lunar and Planetary Science Conference, Lunar and Planetary Science Conference*, 1954  
 Preusker, F., Scholten, F., Matz, K. D., et al. 2017, *A&A*, 607, L1  
 Preusker, F., Scholten, F., Matz, K. D., et al. 2016b, *NASA Planetary Data System, DAWN*  
 Prieto, J. L., Shappee, B. J., Brimacombe, J., et al. 2017, *The Astronomer's Telegram*, 10597, 1  
 Ricker, G. R., Winn, J. N., Vanderspek, R., et al. 2015, *Journal of Astronomical Telescopes, Instruments, and Systems*, 1, 014003  
 Shappee, B. J., Prieto, J. L., Grupe, D., et al. 2014, *ApJ*, 788, 48  
 Slivan, S. M. 2002, *Nature*, 419, 49  
 Szabó, R., Pál, A., Sárneczky, K., et al. 2016, *A&A*, 596, A40  
 Tonry, J. L., Denneau, L., Heinze, A. N., et al. 2018, *PASP*, 130, 064505  
 Udalski, A. 2003, *Acta Astron.*, 53, 291  
 Durech, J., Tonry, J., Erasmus, N., et al. 2020, *A&A*, 643, A59  
 van Buitenen, G., Crinklaw, G., Lutkenhoner, B., et al. 2018, *Minor Planet Electronic Circulars*, 2018-O01  
 Vernazza, P., Brož, M., Drouard, A., et al. 2018, *A&A*, 618, A154  
 Viikinkoski, M., Hanuš, J., Kaasalainen, M., Marchis, F., & Durech, J. 2017, *A&A*, 607, A117  
 Viikinkoski, M., Vernazza, P., Hanuš, J., et al. 2018, *A&A*, 619, L3  
 Vokrouhlický, D., Breiter, S., Nesvorný, D., & Bottke, W. F. 2007, *Icarus*, 191, 636  
 Vokrouhlický, D., Nesvorný, D., & Bottke, W. F. 2003, *Nature*, 425, 147  
 Warner, B. D., Harris, A. W., & Pravec, P. 2009, *Icarus*, 202, 134  
 Watanabe, S., Hirabayashi, M., Hirata, N., et al. 2019, *Science*, 364, 268  
 Woźniak, P. R., Vestrand, W. T., Akerlof, C. W., et al. 2004, *AJ*, 127, 2436

## Appendix A: Additional tables

**Table A.1.** Example of data stored at the CDS (Strasbourg astronomical Data Center). The table provides each asteroid's number and name, the Julian date, the *V* band magnitude and uncertainty, and a flag indicating whether the datapoint was used in the light curve inversion (1 for yes, 0 for no).

Number	Name	JD	<i>V</i> mag	<i>V</i> mag unc	CI flag
1	Ceres	2456598.148220	9.009	0.002	1
1	Ceres	2456601.147060	9.151	0.002	1
1	Ceres	2456619.125000	9.306	0.002	1
1	Ceres	2456622.110740	9.189	0.002	1
1	Ceres	2456625.116330	8.933	0.002	1
1	Ceres	2456626.113730	9.029	0.002	1
1	Ceres	2456642.077830	9.117	0.002	1
1	Ceres	2456657.056800	8.865	0.002	1
1	Ceres	2456659.085710	8.914	0.002	1
1	Ceres	2456675.054510	8.859	0.002	1
1000	Piazzi	2455937.957240	17.015	0.205	0
1000	Piazzi	2455999.891650	16.677	0.105	1
1000	Piazzi	2456003.909970	17.154	0.131	1
1000	Piazzi	2456319.039560	15.460	0.059	1
1000	Piazzi	2456326.080760	15.373	0.044	1
1000	Piazzi	2456336.952390	15.010	0.029	1
1000	Piazzi	2456344.986530	15.137	0.041	1
1000	Piazzi	2456354.835490	14.700	0.026	1
1000	Piazzi	2456359.880710	14.484	0.024	1
1000	Piazzi	2456360.887700	14.424	0.024	1
1000	Piazzi	2456371.931610	14.352	0.023	1
1000	Piazzi	2456991.695440	16.886	0.173	0
1000	Piazzi	2457013.694630	16.538	0.201	0
1000	Piazzi	2457183.116350	16.350	0.190	0

**Table A.2.** Physical properties of asteroids with new shape model determinations based on the *V* band ASAS-SN data.

Asteroid	$\lambda_1$ [deg]	$\beta_1$ [deg]	$\lambda_2$ [deg]	$\beta_2$ [deg]	$P$ [hours]	M	$N_A$	$P_{LCDB}$ [hours]	D [km]
59 Elpis	300	-55			13.6747	CE	289	13.67	3 165.1
70 Panopaea	40	26	233	24	15.8041	C	314	15.81	3 127.9
74 Galatea	109	1	289	14	17.2675	C	327	17.27	3 113.1
83 Beatrix	182	-9			10.1107	E	351	10.16	3 89.6
105 Artemis	47	24			37.118	C	405	37.15	3 119.0
106 Dione	57	12	237	1	16.2126	C	379	16.21	3 153.4
126 Velleda	120	46	300	32	5.36708	C	249	5.37	3 43.9
131 Vala	58	34	244	17	5.18072	C	368	5.18	3 31.3
133 Cyrene	155	-59	348	-52	12.7086	CE	303	12.71	3 72.2
134 Sophrosyne	100	35	276	7	17.1893	CE	293	17.20	3 112.2
137 Meliboea	173	-7	355	13	25.673	C	316	25.68	3 128.7
139 Juewa	96	-1	271	-25	20.9846	C	279	20.99	3 151.1
140 Siwa	88	-27	265	-27	34.398	CE	320	34.45	3 110.6
168 Sibylla	108	-62			47.015	CE	348	47.01	3 145.4
240 Vanadis	64	12	247	16	10.5606	C	349	10.64	3 87.9
248 Lameia	116	18	292	27	11.9120	C	332	11.91	3 50.1
261 Prymno	150	46	334	34	7.9998	C	327	8.00	3 50.0
326 Tamara	76	7			14.4613	CE	306	14.45	3 89.4
342 Endymion	82	-9			6.31652	CE	336	6.32	3 64.3
356 Liguria	57	-33			31.705	C	357	31.70	3 118.5
370 Modestia	168	-69	323	-64	22.5400	CE	301	22.53	3 38.1
408 Fama	81	37	280	19	202.64	C	328	202.10	3 35.6
415 Palatia	329	-25			20.7313	CE	325	20.73	3 83.6
432 Pythia	332	-64			8.2509	CE	330	8.25	3 46.8
438 Zeuxo	21	-4			8.8317	C	300	8.83	3 58.9
447 Valentine	168	-61	358	-82	9.6528	CE	304	9.65	3 85.2
475 Occko	191	38			7.3151	C	219	7.32	3 18.6
476 Hedwig	56	46	227	20	27.240	C	305	27.33	3 111.1
481 Emita	6	38	306	69	14.4495	CE	328	14.41	3 103.5
483 Seppina	352	60			12.7211	CE	313	12.73	3 66.9
496 Gryphia	141	26	325	36	1049.0	CE	218	1072.00	3 10.9
498 Tokio	102	-24	275	-10	41.865	CE	354	41.85	3 86.0
514 Armida	22	14	199	6	21.8756	CE	296	21.85	3 97.3
524 Fidelio	195	51	357	57	14.1708	E	302	14.20	3 65.5
530 Turandot	38	15	217	32	19.9537	C	233	19.96	3- 88.4
535 Montague	22	-71	187	-57	10.2512	C	302	10.25	3 78.1
542 Susanna	126	-79			10.0856	CE	359	10.07	3 42.1
552 Sigelinde	26	62	196	46	17.1498	CE	250	17.16	3 77.7
554 Peraga	82	-55	260	-42	13.7120	C	292	13.71	3 97.0
575 Renate	252	31			3.67614	C	240	3.68	3 19.1
599 Luisa	87	49			9.5645	C	336	9.57	3 70.2
627 Charis	152	62	350	41	27.895	CE	299	27.89	3 38.0
633 Zelima	53	-37	233	-1	11.7298	E	288	11.73	3 33.4
671 Carnegia	61	16	245	1	8.3306	CE	274	8.33	3- 69.3
716 Berkeley	164	40	351	37	15.5747	CE	310	15.55	2+ 19.8
740 Cantabia	156	-44	312	-51	64.317	CE	331	64.45	3 91.6
751 Faina	158	25	339	-10	23.673	CE	310	23.68	3 113.7
773 Irmtraud	27	21	210	-14	6.7484	C	344	6.75	3 87.1
786 Bredichina	54	-11	236	18	29.849	CE	350	29.43	3- 105.3
945 Barcelona	305	44			7.4187	C	289	7.36	3 26.7
949 Hel	104	-43			16.4381	C	303	8.21	2+ 63.5
971 Alsatia	85	-57	219	-46	9.6066	E	264	9.61	3 60.9
974 Lioba	65	-13	242	-8	309.2	C	264	38.70	3 21.8
988 Appella	54	32	237	32	948.0	C	98	120.00	2 20.4
1003 Lilofee	29	63	223	59	8.2499	CE	249	8.26	3 33.7
1044 Teutonia	124	55	311	46	3.15691	E	254	3.15	3 17.5
1046 Edwin	97	8	278	-6	5.29077	C	223	5.29	3 29.1
1047 Geisha	47	78	257	74	25.686	CE	213	25.62	3- 10.7
1048 Feodosia	320	-47			10.4242	CE	349	10.46	2 85.1

**Table A.2.** continued.

Asteroid	$\lambda_1$ [deg]	$\beta_1$ [deg]	$\lambda_2$ [deg]	$\beta_2$ [deg]	P [hours]	M	$N_A$	$P_{LCDB}$ [hours]	D [km]
1059 Mussorgskia	145	25	335	43	5.63412	CE	231	5.64	3 25.2
1071 Brita	180	13	358	5	5.81674	C	303	5.82	3 62.5
1139 Atami	270	-29			27.473	E	200	27.45	3 8.2
1166 Sakuntala	177	52	360	-20	6.29174	C	220	6.29	3 26.0
1168 Brandia	152	-76	324	-24	11.4468	CE	86	11.44	3 10.1
1193 Africa	209	84	328	51	157.92	CE	181	158.70	2+ 12.2
1235 Schorria	103	-59			1304.1	CE	145	1265.00	3 6.4
1243 Pamela	111	58			26.011	CE	295	26.02	2 69.9
1304 Arosa	159	-18	319	-63	7.7481	CE	329	7.75	3 43.6
1325 Inanda	54	55	249	50	138.76	E	132	20.52	2 10.5
1326 Losaka	171	-32	298	-47	276.1	E	270	6.90	2 26.3
1358 Gaika	76	38	258	29	10.1405	E	171		23.1
1447 Utra	70	2	250	-4	179.14	C	213	257.00	2 11.8
1481 Tubingia	58	90	252	69	248.2	E	295	24.00	2 33.8
1523 Pieksamaki	18	51	207	37	5.32033	C	183	5.32	3 9.1
1532 Inari	254	28			264.5	CE	157	25.00	1+ 24.4
1536 Pielinen	26	-60	219	-61	66.267	C	196	66.22	3 8.0
1558 Jarnefelt	10	-28	192	-5	6.25728	C	301	6.25	2 61.8
1575 Winifred	305	-46			123.85	CE	186	125.00	3 9.5
1594 Danjon	64	60	283	55	122.73	CE	251	12.00	1 10.5
1675 Simonida	147	59	316	29	5.28808	C	240	5.29	3 12.2
1784 Benguella	146	63	323	69	133.18	CE	198		10.5
1795 Woltjer	155	-9	335	0	13.2288	E	101	12.10	2+ 23.9
1806 Derice	30	19	208	5	3.22397	E	200	3.22	3 8.0
1886 Lowell	107	-52	135	-88	159.02	E	182		
2021 Poincare	90	14	276	33	4.40548	C	71	4.41	3 5.0
2035 Stearns	103	25			93.84	E	264	93.00	2+ 7.6
2089 Cetacea	24	66			208.39	CE	207	39.12	2 17.7
2105 Gudy	351	-22			15.8094	CE	235	15.79	3- 19.7
2118 Flagstaff	126	57	288	47	15.1684	CE	160	15.17	3- 11.4
2126 Gerasimovich	52	62	242	52	1296.5	E	162	22.95	2 7.8
2163 Korczak	9	12	189	17	3.98378	C	127	4.00	2 24.4
2234 Schmadel	49	9	212	-37	15.8126	C	112	15.63	2+ 9.5
2263 Shaanxi	67	-73	186	-63	275.8	E	142	41.70	2- 22.3
2364 Seillier	44	53	250	40	24.201	C	186	12.28	2+ 19.6
2376 Martynov	28	-69	216	-56	11.1374	E	218		41.6
2443 Tomeileen	97	-28	264	-12	7.9540	CE	244	3.97	2 31.9
2453 Wabash	93	-35	269	-58	6.87965	CE	209	6.88	3 19.2
2678 Aavasaksa	88	72	282	61	82.21	CE	164	82.20	3- 8.4
2698 Azerbajdzhana	197	-77	309	-90	27.362	E	163	27.20	3- 14.8
2732 Witt	98	-80	255	-64	12.6244	CE	143	12.62	2 11.0
2813 Zappala	257	75			18.2222	CE	227	18.23	3 32.0
2853 Harvill	85	-55	265	-42	6.30440	CE	110	6.30	3- 7.0
2912 Lapalma	191	-72	281	-90	5.71085	C	147	5.71	3 6.5
3109 Machin	102	-49	254	-80	20.2904	C	181	20.30	2 23.7
3227 Hasegawa	64	-26	244	-15	6.5364	E	113	6.54	3 7.9
3233 Krisbarons	136	-36	319	-51	886.8	E	103	888.00	2 4.1
3300 McGlasson	45	67	284	54	50.124	E	284	22.91	2 22.8
3395 Jitka	11	53	204	50	18.2860	C	133	18.29	3 10.9
3403 Tammy	130	-35	311	-32	128.26	CE	101	11.85	1 4.1
3438 Inarradas	102	-62	324	-58	24.891	E	90	24.82	2 25.3
3575 Anyuta	131	-42	292	-55	6.32044	CE	138	6.32	3 11.7
3682 Welther	96	60	179	60	3.59730	C	143	3.60	3 19.1
3915 Fukushima	180	-71	275	-65	9.4199	CE	210	9.42	3 21.3
3995 Sakaino	14	59	172	90	4.55238	CE	133	4.55	3 9.5
4002 Shinagawa	99	-86	264	-85	174.00	CE	223	175.00	3- 10.0
4024 Ronan	340	71			354.0	C	98	356.00	3- 11.9
4116 Elachi	292	-7			38.190	C	90	38.14	3 4.7
4142 Dersu-Uzala	175	-19			272.0	E	124	276.00	2 6.3
4154 Rumsey	122	17	304	-1	3.25709	E	64	3.26	3 6.2

**Table A.2.** continued.

Asteroid	$\lambda_1$ [deg]	$\beta_1$ [deg]	$\lambda_2$ [deg]	$\beta_2$ [deg]	$P$ [hours]	M	$N_A$	$P_{LCDB}$ [hours]	D [km]	
4298 –	244	-15			30.557	E	68	30.47	2	16.5
4327 Ries	59	93	321	65	125.99	CE	155	126.56	2	14.4
4437 Yaroshenko	36	-47	233	-53	29.576	E	100	30.00	1+	4.7
4451 Grieve	111	-77			6.86015	E	108	6.86	3	15.5
4614 Masamura	86	58	253	41	191.46	E	118	14.40	1	6.1
4698 Jizera	122	70	275	61	158.54	E	73			4.4
4771 Hayashi	26	-50	210	-68	9.8036	E	82	9.80	3-	12.7
5064 Tanchozuru	262	-77			457.7	E	80	8.13	2-	4.8
5081 Sanguin	70	-77	292	-89	10.2644	E	120	10.26	3	17.5
5563 –	120	-1	292	-28	3.22186	C	142	3.22	3-	10.2
5595 Roth	128	-8	293	-15	468.2	C	115			9.8
5597 Warren	59	-31	232	-48	73.20	E	81			4.0
5651 Traversa	17	64	113	66	470.1	E	124			32.1
5746 –	209	-37	250	-12	267.3	E	77			
5747 –	66	44	231	-6	196.77	CE	98	196.45	2+	9.3
5849 –	226	-58	315	-90	8.7328	CE	241	8.73	3	30.4
5851 –	46	-70			367.0	E	114	367.50	3	
5855 Yukitsuna	196	79	281	62	19.3147	CE	135	19.04	2+	11.1
5977 –	50	61			42.439	CE	156			11.4
6223 Dahl	25	71	207	64	3.33441	E	69	3.33	2	19.6
6349 Acapulco	53	20	233	-8	23.8123	C	123	4.38	2	20.4
6354 Vangelis	59	-61	187	-31	4.03925	E	97	4.04	3-	10.3
7021 –	166	-15	338	-53	6.2680	E	100			
7055 –	165	-50			4.16882	E	70	4.17	3	6.7
7102 –	102	-39	323	-26	6.1784	E	79			21.4
7295 –	284	37			3.34688	E	66	3.35	3	
7641 –	88	-5	256	18	27.762	C	68	27.77	3	75.3
8059 Deliyannis	156	70	331	37	6.00421	E	185	6.00	3-	12.0
8278 –	135	-47	298	-74	75.06	E	98			9.6
9442 –	80	12			5.37555	E	80			6.7
11861 –	51	-83	201	-86	4.89689	E	150			11.7
13123 Tyson	331	-46	331	-51	3.32948	E	124	3.33	3	10.9
13165 –	57	65	241	54	64.198	E	65			4.3
13351 Zibeline	96	4	275	28	232.0	E	70			3.8
13488 Savanov	51	-50	254	-43	5.67938	E	75	5.68	2	14.4
13538 –	227	-44			12.3203	E	88	12.32	3	4.8
16018 –	91	33	248	29	207.41	E	86	24.00	1	19.3
16528 Terakado	192	-69	238	-5	23.381	E	68	23.38	2+	8.2
16592 –	8	9	186	-19	154.07	C	122	137.69	2	10.5
17770 Baume	62	-25	239	5	3.2638	E	60	3.26	2	5.7
31450 –	84	37	260	9	3.41110	C	75	3.41	3	10.6
31889 –	76	15	270	2	123.6	E	61			10.4
40429 –	46	-36	205	-21	404.2	C	64	24.00	1	9.3
93768 –	85	-7	350	-8	2.6812	E	63	2.68	3	3.1

**Notes.** We provide ecliptic coordinates  $\lambda$  and  $\beta$  of up to two pole solutions, sidereal rotational period  $P$  (its uncertainty is on the order of the last digit). The method column (M) indicates whether the rotation period was derived by the convex inversion approach (C), the ellipsoid approach (E), or both (CE). The final columns are the number of ASAS-SN measurements  $N_A$ , the LCDB period with its reliability flag (Warner et al. 2009), and the size  $D$  from the MP3C database<sup>3</sup>.

**Table A.3.** Physical properties of asteroids with new shape model determinations based on the V band ASAS-SN data.

Asteroid	$\lambda_1$ [deg]	$\beta_1$ [deg]	$\lambda_2$ [deg]	$\beta_2$ [deg]	$P$ [hours]	M	$N_A$	$P_{LCDB}$ [hours]	D [km]	$\lambda_D$ [deg]	$\beta_{D1}$ [deg]	$\lambda_{D2}$ [deg]	$\beta_{D2}$ [deg]	$P_D$ [hours]	
5 Astraea	84	52	270	44	16.8006	CE	312	16.81	3	108.3	124	39		16.8006	
12 Victoria	170	37			8.6604	C	347	8.66	3	115.1	178	-28		8.6603	
13 Egeria	34	46			7.046664	C	262	7.04	3	227.0	54	34	233	6	7.046667
16 Psyche	35	-11	215	16	4.19597	C	377	4.20	3	207.2	36	-10		4.19595	
17 Thetis	55	12	237	21	12.2660	CE	290	12.27	3	84.9	236	19		12.2660	
19 Fortuna	102	51	283	59	7.4432	CE	252	7.44	3	196.4	97	69		7.4432	
20 Massalia	122	46	302	47	8.0976	CE	312	8.10	3	131.6	179	39	360	40	8.0990
21 Lutetia	52	-3	232	-0	8.1683	CE	300	8.17	3	108.4	52	-6		8.1683	
23 Thalia	340	-70			12.3122	CE	304	12.31	3	106.2	158	-46	343	-74	12.3124
25 Phocaea	342	9			9.9353	CE	334	9.93	3	83.2	347	10		9.9354	
28 Bellona	103	-10	282	4	15.7078	CE	362	15.71	3	97.4	98	-10		15.7079	
30 Urania	104	18	283	15	13.6870	C	346	13.69	3	92.8	107	23	284	20	13.6872
31 Euphrosyne	95	68	289	-11	5.52964	C	280	5.53	3	259.9	92	68		5.52959	
32 Pomona	86	46	255	50	9.4476	CE	241	9.45	3	81.8	267	58		9.4477	
34 Circe	97	45	277	72	12.1746	CE	301	12.15	3	115.5	94	35	275	51	12.1746
36 Atalante	27	-42	194	16	9.9269	E	336	9.93	3	103.0	190	-55	45	-49	9.9269
37 Fides	90	30	271	26	7.3325	CE	333	7.33	3	103.2	270	19		7.3325	
38 Leda	156	-38			12.8360	CE	317	12.84	3	92.2	161	-15	345	-4	12.8361
39 Laetitia	335	38			5.13822	CE	303	5.14	3	179.5	323	33		5.13824	
40 Harmonia	26	42	214	48	8.9085	C	375	8.91	3	111.2	22	38		8.9085	
41 Daphne	206	-28			5.98796	E	311	5.99	3	179.6	200	-32		5.98798	
42 Isis	109	44	301	38	13.5835	CE	335	13.59	3	104.5	108	44		13.5836	
43 Ariadne	254	-14			5.76202	CE	316	5.76	3	71.3	251	-10		5.76199	
44 Nysa	98	42	283	50	6.42144	CE	318	6.42	3	75.7	101	51		6.42142	
48 Doris	104	37	288	51	11.8901	CE	326	11.89	3	216.5	298	59		11.8901	
54 Alexandra	148	16	320	20	7.02266	CE	315	7.02	3	142.0	154	17		7.02264	
62 Erato	89	17	271	21	9.2183	CE	349	9.22	3	78.6	87	22	269	23	9.2182
63 Ausonia	119	-27			9.2976	CE	377	9.30	3	91.6	120	-15		9.2976	
64 Angelina	317	6			8.7517	CE	332	8.75	3	58.3	317	17	138	14	8.7503
67 Asia	330	82			15.8507	CE	260	15.85	3	56.3	117	42	286	50	15.8504
68 Leto	118	66			14.8453	C	303	14.85	3	122.5	103	43		14.8455	
69 Hesperia	84	3	264	19	5.65524	C	313	5.66	3	132.7	250	17	71	-2	5.65534
71 Niobe	89	-35			35.853	C	276	35.86	3	82.0	88	-33		35.852	
72 Feronia	84	-24	268	-22	8.0907	CE	252	8.10	3	78.8	98	-52		8.0907	
76 Freia	131	-10	310	-8	9.9731	CE	313	9.97	3	145.4	140	14	320	17	9.9731
80 Sappho	197	-23			14.0309	CE	390	14.03	3	74.2	196	-21		14.0309	
82 Alkmene	170	-30	355	-36	13.0008	CE	288	13.00	3	57.6	164	-28	349	-33	13.0008
84 Klio	359	-56			23.5736	C	338	23.56	3	79.0	356	-53		23.5750	
85 Io	116	-46	294	-18	6.87485	CE	287	6.88	3	169.5	92	-68		6.87478	
86 Semele	53	-45	226	-39	16.6420	C	339	16.63	3	109.9	213	-31	44	-43	16.6420
87 Sylvia	63	66	285	53	5.18364	CE	332	5.18	3	253.1	72	68		5.18364	
89 Julia	16	-22			11.3883	CE	304	11.39	3	145.5	14	-24		11.3883	

Table A.3. continued.

Asteroid	$\lambda_1$ [deg]	$\beta_1$ [deg]	$\lambda_2$ [deg]	$\beta_2$ [deg]	$P$ [hours]	M	$N_A$	$P_{LCDB}$ [hours]	D [km]	$\lambda_D$ [deg]	$\beta_{D1}$ [deg]	$\lambda_{D2}$ [deg]	$\beta_{D2}$ [deg]	$P_D$ [hours]	
91 Aegina	202	36	313	65	6.02831	CE	226	6.03	3	103.4	40	32	218	36	6.02819
95 Arethusa	139	37	29	5	8.7022	CE	272	8.71	3	149.1	149	33	35.251	8.7022	
97 Klotho	7	36	288	62	35.251	CE	364	35.15	3	100.7	359	30	16.4801	16.4801	
98 Ianthe	115	35	228	52	16.4803	CE	263	16.48	3	102.5	286	18	18.1191	18.1191	
99 Dike	5	46	303	52	18.1190	CE	337	18.13	3	67.3	233	50	27.070	27.070	
100 Hekate	105	78	62	52	27.071	CE	309	27.07	3	85.7	306	52	104	104	
107 Camilla	76	12	255	1	4.84393	CE	359	4.84	3	210.4	76	55	4.84393	4.84393	
109 Felicitas	108	-58	296	-59	31.463	CE	373	31.47	3	69.8	286	-50	101	-66	
112 Iphigenia	156	-40	292	-54	10.7434	C	193	10.74	3	94.2	196	-55	5	-59	
114 Cassandra	48	-57	218	-53	12.0325	CE	330	12.03	3	78.3	51	-53	222	-53	
116 Sirona	118	-35	9.1242	C	264	9.13	3	161.6	117	-19	323	-57	57	9.1242	
117 Lomia	182	68	347	39	7.8064	CE	326	7.81	3	40.2	346	34	176	59	
118 Peitho	1	-59	205	-67	11.4651	CE	360	11.48	3	59.3	339	-67	181	-61	
119 Althea	97	44	267	16	46.541	C	296	46.55	3	155.1	256	39	82	55	
120 Lachesis	4	17	187	28	5.55087	CE	325	5.55	3	166.2	359	8	3	15	
121 Hermione	21	14	199	16	10.6872	CE	293	10.69	3	70.7	23	20	201	22	
122 Gerda	77	54	245	41	9.8734	CE	332	9.87	3	48.2	242	38	78	51	
123 Brunhild	28	72	204	83	3.96820	CE	318	3.97	3	48.4	95	68	280	74	
125 Libertatrix	90	-54	12.7994	CE	326	12.80	3	114.2	98	-60	261	-70	12.7995	12.7995	
127 Johanna	220	64	4.95717	CE	307	4.96	3	128.7	205	63	60	60	60	4.95716	
129 Antigone	7	-95	5.22466	CE	319	5.22	3	180.7	64	-90	261	-70	261	5.22466	
130 Elektra	300	81	5.16824	C	373	5.17	3	44.5	326	67	67	67	67	5.16827	
132 Aethra	138	-66	189	-61	10.1030	CE	226	10.10	3	52.9	49	-42	222	-39	
147 Protageneia	92	10	272	11	7.8523	CE	354	7.85	3	108.4	90	14	269	15	
148 Gallia	147	-37	20.6642	C	343	20.66	3	80.9	140	-17	17	17	17	20.6636	
151 Abundantia	187	21	9.8637	C	308	9.86	3	39.0	188	32	3	3	16	9.8643	
152 Atala	29	53	224	61	6.2447	CE	339	6.25	3	59.0	347	47	47	6.2447	
156 Xanthippe	32	37	202	24	22.116	CE	394	22.13	3	123.7	197	9	22	22	
158 Koronis	9	-57	189	-60	14.2057	CE	286	14.22	3	39.0	30	-64	348	59	
159 Aenilia	120	71	322	54	24.479	CE	310	24.48	3	125.2	139	68	348	59	
161 Athor	357	-13	13.6639	C	268	7.28	3	40.8	350	350	-6	170	4	7.8523	
164 Eva	54	-15	40	6.66537	CE	341	6.67	3	105.0	144	-10	170	4	13.6638	
171 Ophelia	150	48	333	40	5.75026	CE	350	5.74	3	64.8	266	29	329	23	
174 Phaedra	89	32	264	9	8.3280	E	291	8.32	3	111.9	28	89	20	8.3280	
175 Andromache	125	73	269	28	12.3214	C	248	12.32	3	38.3	79	9	260	20	
178 Belisana	87	26	11.1733	CE	272	11.17	3	70.0	248	-9	65	-6	6	12.3214	
179 Klytaemnestra	68	-7	41	11.9765	CE	287	11.98	3-	35.8	32	48	48	48	11.1734	
183 Istra	85	16	11.7686	CE	307	11.77	3	32.3	85	20	20	20	20	11.7690	
184 Dejopeja	16	41	39	6.44109	CE	337	6.44	3	62.5	200	52	52	52	6.44111	
186 Celuta	101	-59	139	-55	19.843	CE	314	19.84	3	235	-77	88	88	-54	
188 Menippe	34	53	191	-43	17.6035	CE	274	17.60	3	94.5	170	-39	328	-42	
191 Kolga	196	-39	360	-43	17.6035	CE	274	17.60	3	94.5	170	-39	328	-42	

Table A.3. continued.

Asteroid	$\lambda_1$ [deg]	$\beta_1$ [deg]	$\lambda_2$ [deg]	$\beta_2$ [deg]	$P$ [hours]	M	$N_A$	$P_{LCDB}$ [hours]	D [km]	$\lambda_D$ [deg]	$\beta_{D1}$ [deg]	$\lambda_{D2}$ [deg]	$\beta_{D2}$ [deg]	$P_D$ [hours]	
193 Ambrosia	138	-6	321	-13	6.58177	CE	329	6.58	3	26.3	141	-11	328	-17	6.58167
195 Eurykleia	303	41			16.5219	C	353	16.52	3	85.3	101	71	352	83	16.5218
196 Philomela	272	-47			8.3328	C	314	8.33	3	144.6	111	-41	276	-49	8.3328
201 Penelope	82	-45	260	-32	3.74744	CE	339	3.75	3	85.9	84	-15			3.74746
204 Kallisto	37	43	197	46	19.4867	C	380	19.49	3	48.6	188	14	15	30	19.4870
208 Lacrimosa	20	54	204	58	14.0856	CE	305	14.09	3	40.9	202	61	16	60	14.0857
209 Dido	40	-29	211	-36	5.73558	CE	337	5.74	3	118.4	217	-39	43	-34	5.73561
210 Isabella	103	-12	279	-15	6.6719	C	327	6.67	3	69.6	278	-26	100	-14	6.6719
216 Kleopatra	70	11			5.38525	CE	302	5.38	3	119.2	74	20			5.38528
218 Bianca	122	5	308	27	6.33717	C	305	6.34	3	57.3	305	17			6.33717
219 Thusnelda	219	-42	260	-68	59.709	C	273	59.74	3	37.7	253	-69			59.712
222 Lucia	102	49	288	49	7.8367	C	296	7.84	3	55.4	293	49	106	50	7.8367
225 Henrietta	188	49			7.3561	CE	335	7.36	3	95.9	184	54			7.3561
226 Weringia	282	-19			11.1485	C	295	11.15	3	31.5	284	-14			11.1485
231 Vindobona	38	79	236	68	14.2447	C	244	14.24	3	73.5	223	49			14.2447
232 Russia	14	-46	206	-44	21.9064	CE	313	21.91	3	54.7	198	-31	3	-45	21.9071
233 Asterope	295	61			19.6980	CE	362	19.70	3	99.7	318	61			19.6980
234 Barbara	161	-53	306	-33	26.474	CE	278	26.47	3	45.5	166	-38	318	-36	26.480
237 Coelestina	30	9	213	21	29.176	CE	296	29.21	3	39.5	230	30	42	14	29.175
238 Hypatia	95	-20	276	4	8.8747	C	323	8.87	3	155.7	261	45	84	20	8.8727
239 Adrastea	214	-81	346	-63	18.4719	CE	239	18.47	3	37.6	226	-70			18.4717
242 Kriemhild	101	-45			4.54516	C	356	4.55	3	40.8	284	-15	100	-40	4.54518
243 Ida	66	-62	246	-63	4.63364	CE	410	4.63	3	29.0	259	-66	74	-61	4.63363
244 Sita	183	-74	280	-79	129.71	CE	175	129.51	3-	11.1	41	-80	218	-74	129.72
245 Vera	94	-30			14.3560	C	359	14.38	3	76.0	96	-50	265	-51	14.3565
246 Asporina	230	-27			16.2523	C	309	16.22	3	50.9	235	-10	47	-36	16.2522
247 Eukrate	97	-26	277	27	12.0957	E	365	12.09	3	130.9	103	-22			12.0948
250 Bettina	103	20	284	-9	5.05441	C	317	5.05	3	121.0	99	10			5.05441
253 Mathilde	179	-67	350	-46	420.2	CE	367	417.70	3	54.0	334	-65			420.1
257 Silesia	2	-47	175	-44	15.7097	CE	307	15.71	3	79.2	5	-53	176	-46	15.7097
258 Tyche	56	20			10.0401	CE	399	10.04	3	64.4	224	-4	40	-9	10.0401
260 Huberta	24	-32	210	-24	8.2905	CE	287	8.29	3	101.5	206	-19	23	-28	8.2905
262 Valda	3	36	196	49	17.3856	C	195	17.39	3	14.7	186	27	1	17	17.3854
265 Anna	106	-66	336	-68	11.6903	CE	163	11.68	3	26.5	109	-53			11.6903
267 Tirza	102	-31	275	-37	7.6528	CE	313	7.65	3	56.4	268	-45	99	-38	7.6529
269 Justitia	80	-77	251	-59	33.129	CE	387	33.13	3	50.7	71	-79	251	-69	33.129
271 Penthesilea	43	64	229	60	18.7873	CE	306	18.79	3	69.0	225	49	42	53	18.7875
272 Antonia	140	-77	231	-93	3.85480	CE	289	3.85	3	26.9	293	-90			3.85480
273 Atropos	260	-43			23.928	CE	301	23.92	3	29.8	250	-38			23.928
274 Philagoria	125	-80	242	-56	17.9408	CE	332	17.94	3	27.3	274	-78	114	-66	17.9408
278 Paulina	117	50	304	36	6.49386	CE	345	6.50	3	32.8	307	31	118	38	6.49387
283 Emma	79	24	255	10	6.8952	CE	375	6.90	3	132.4	257	23			6.8952
287 Nephthys	153	28	345	24	7.6040	C	267	7.61	3	59.6	356	36	158	39	7.6041

Table A.3. continued.

Asteroid	$\lambda_1$ [deg]	$\beta_1$ [deg]	$\lambda_2$ [deg]	$\beta_2$ [deg]	$P$ [hours]	M	$N_A$	$P_{LCDB}$ [hours]	D [km]	$\lambda_D$ [deg]	$\beta_{D1}$ [deg]	$\lambda_{D2}$ [deg]	$\beta_{D2}$ [deg]	$P_D$ [hours]	
290 Bruna	94	-9	234	-82	13.8054	CE	210	13.81	3	9.8	37	-74	286	-80	13.8056
292 Ludovica	106	38	295	6	8.9263	CE	216	8.93	3	30.9	110	39	289	-2	8.9263
297 Caecilia	49	-43	223	-53	4.15138	CE	314	4.16	3	42.3	223	-53	47	-33	4.15139
301 Bavaria	54	55	224	58	12.2408	CE	289	12.25	3	53.0	226	70	46	61	12.2409
302 Clariissa	106	-82	350	-66	14.4766	CE	258	14.38	3	34.4	28	-72	190	-72	14.4767
304 Olga	31	26	185	52	18.2016	C	264	18.36	3	66.0	38	37			18.2012
306 Unitas	77	-53	251	-33	8.7388	CE	265	8.74	3	47.2	79	-35	253	-17	8.7387
310 Margarita	38	-26	222	-34	12.0708	E	273	12.07	3	33.7	225	-35	42	-33	12.0710
311 Claudia	28	42	213	52	7.5314	CE	272	7.53	3	26.3	30	40	214	43	7.5314
312 Pierretta	73	-43	245	-59	10.2076	CE	323	10.28	3	46.2	82	-39	256	-58	10.2076
317 Roxane	148	-98	324	-83	8.1696	CE	304	8.17	3	18.6	220	-62	40	-70	8.1696
321 Florentina	100	-40	273	-61	2.87086	CE	293	2.87	3	28.0	95	-60	267	-66	2.87087
327 Columbia	52	59	242	40	5.93186	CE	315	5.93	3	26.2	238	26	52	43	5.93183
328 Gudrun	29	9			10.9849	CE	307	10.99	3	116.8	31	11	210	-15	10.9851
329 Svea	25	46			22.7667	C	329	22.78	3-	74.1	33	51			22.7670
332 Siri	72	49	256	39	8.0062	C	311	8.01	3	42.5	259	48			8.0062
333 Badenia	12	-50	185	-49	9.8611	CE	374	9.86	3	72.2	5	-54			9.8611
334 Chiciego	13	33	188	44	7.36012	CE	366	7.36	3	174.1	21	20	200	32	7.36014
336 Lacadiera	3	62	171	53	13.6955	C	325	13.70	3	69.0	194	39	37	54	13.6955
337 Devosa	8	40	201	36	4.65278	CE	279	4.65	3	66.6	359	55	163	28	4.65292
338 Budrosa	152	-19	336	-18	4.60781	E	256	4.61	3	50.5	333	-7	151	-22	4.60783
340 Eduarda	19	-40	190	-44	8.0061	CE	306	8.01	3	28.0	188	-43	18	-47	8.0061
345 Tercidina	157	-46			12.3710	C	241	12.37	3	99.0	346	-55			12.3708
347 Pariana	44	22	237	38	4.05244	E	279	4.05	3	48.6	41	2	230	25	4.05246
349 Dembowska	327	14			4.70119	CE	303	4.70	3	126.8	322	18			4.70120
350 Ornamenta	188	-13			9.1805	C	333	9.18	3	121.4	184	-29			9.1804
352 Gisela	22	-30	206	-34	7.4801	C	288	7.49	3	26.7	24	-21	206	-28	7.4801
354 Eleonora	134	50			4.27720	CE	332	4.28	3	149.0	156	45			4.27719
355 Gabriella	116	107	295	67	4.82898	CE	289	4.83	3	24.0	341	83	159	88	4.82899
360 Carlova	16	71	132	64	6.18957	CE	327	6.18	3	129.1	355	55			6.18959
361 Bononia	99	58	281	30	13.8064	C	313	13.84	3	151.8	115	45	294	13	13.8063
365 Corduba	79	13			12.7052	C	289	12.71	3	86.8	80	4	255	33	12.7055
367 Amictia	28	36	209	48	5.05501	CE	278	5.06	3	16.8	203	38	21	32	5.05502
373 Melusina	146	-47			12.9864	CE	341	12.97	3	93.0	147	-61	19	-48	12.9863
374 Burgundia	14	44			6.96401	C	372	6.97	3	52.8	13	41	180	23	6.96394
377 Campania	42	66	193	57	11.6644	CE	311	11.66	3	90.3	47	67	196	66	11.6644
381 Myrrha	50	32	260	82	6.57197	CE	335	6.57	3	127.6	31	44	228	79	6.57195
385 Ilmatar	235	18			62.523	CE	212	62.35	3	85.8	51	55			62.540
386 Siegena	290	31			9.7652	C	298	9.76	3	201.2	287	25			9.7650
387 Aquitania	144	44			24.1400	C	361	24.14	3	105.1	123	46			24.1401
388 Charybdis	154	71	312	43	9.5112	CE	244	9.52	3	125.8	124	54			9.5112
391 Ingeborg	238	-75	263	-52	26.415	CE	261	26.39	3	18.1	354	-65			26.415
394 Arduna	64	-76	152	-68	16.6217	CE	350	16.53	3	30.0	195	-61	56	-79	16.6217

Table A.3. continued.

Asteroid	$\lambda_1$ [deg]	$\beta_1$ [deg]	$\lambda_2$ [deg]	$\beta_2$ [deg]	$P$ [hours]	M	$N_A$	$P_{LCDB}$ [hours]	D [km]	$\lambda_D$ [deg]	$\beta_{D1}$ [deg]	$\lambda_{D2}$ [deg]	$\beta_{D2}$ [deg]	$P_D$ [hours]
399 Persephone	320	83	9.1464	CE	289	9.14	3	46.3	36	63	231	33	9.1464	
402 Chloe	306	-48	10.6685	CE	326	10.66	3	55.4	160	-37	312	-49	10.6684	
403 Cyane	75	38	12.2701	CE	342	12.28	3	43.8	230	33	65	35	12.2700	
405 Thia	339	44	9.9649	CE	277	10.08	3	108.9	332	45	157	1	9.9650	
406 Erna	4	-60	8.7908	E	258	8.79	3	46.0	357	-49	161	-60	8.7908	
407 Arachne	43	-64	22.626	CE	366	22.63	3	97.5	43	-58	241	-63	22.626	
409 Aspasia	8	29	9.0214	C	384	9.02	3	171.0	4	29			9.0214	
410 Chlois	83	23	276	27	32.497	CE	310	32.50	3	118.9	81	1	261	-1
413 Edburgha	212	-57	15.7715	CE	360	15.77	3	32.5	202	-45			15.7715	
416 Vaticanana	97	28	286	15	5.37159	CE	312	5.37	3	88.8	291	12		5.37160
418 Alemannia	154	-56	336	-49	4.67209	CE	331	4.67	3	40.3	337	-39		4.67211
424 Grania	170	-5	348	-24	20.0610	CE	307	20.07	3-	70.5	351	-24	172	-6
426 Hippo	42	-38	105	-87	67.506	CE	273	34.30	2	133.9	319	-66	14	-57
427 Galene	57	-68	248	-76	3.70603	CE	296	3.71	3	32.2	272	-75	72	-57
433 Eros	20	8			5.27029	CE	159	5.27	3	23.3	17	11		5.27026
435 Ella	54	245	50	50	4.622280	CE	331	4.62	3	37.0	59	64	247	58
441 Bathilde	124	42			10.4432	CE	292	10.45	3	65.5	122	43	285	55
445 Edna	18	-42			19.9767	C	336	19.96	3	87.8	10	-45		19.9764
446 Aeternitas	42	97			15.7374	CE	305	15.74	3	53.6	194	57	356	52
453 Tea	18	16	204	37	6.81032	CE	312	6.81	3	24.0	197	16	11	28
454 Mathesis	134	54			8.3777	CE	285	8.38	3	81.7	147	55	321	28
455 Bruchsalia	71	-20	243	-17	11.8398	C	325	11.85	2+	112.4	73	-21	242	-13
456 Abnoba	59	50			18.2787	CE	344	18.28	3	37.7	58	56		18.2791
458 Herynia	82	13	272	36	21.8123	CE	328	21.81	3	36.7	74	14	262	32
461 Saska	148	-57	325	-56	7.3470	CE	298	7.35	3	43.6	195	-72	11	-70
470 Kilia	77	48	251	65	295.1	CE	350	290.0	2	27.8	196	44		295.0
472 Roma	132	58	354	38	9.7964	CE	384	9.80	3	50.3	118	50		9.7965
474 Prudentia	111	-74	274	-50	8.5722	CE	340	8.57	3	41.0	135	-65	301	-51
478 Tergeste	7	-25	209	-41	16.1028	E	257	16.10	3-	80.7	216	-56		16.1031
480 Hansa	358	15			16.1896	CE	332	16.19	3	55.9	173	-32	352	18
482 Petrina	95	18	273	52	11.7921	E	318	11.79	3	45.8	281	61	94	24
484 Pittsburghia	72	41			10.6500	CE	276	10.63	3	30.1	70	46		10.6498
485 Genua	323	-41			17.6195	CE	338	17.59	3	54.7	322	-50		17.6191
489 Comacina	93	-50	267	-21	9.0232	CE	326	9.02	3	134.6	88	-43	265	-16
490 Veritas	73	56	233	64	7.9282	CE	340	7.93	3	112.8	56	34	231	43
495 Eulalia	38	40	214	43	28.966	CE	247	28.97	3	37.3	212	46	38	35
502 Sigune	176	-38			10.9267	CE	339	10.92	3	15.8	178	-36		10.9267
503 Evelyn	109	-63	250	-85	38.779	CE	323	38.78	3-	90.2	246	-64	89	-56
505 Cava	285	-64			8.1799	C	319	8.18	3	117.7	131	-21	304	-44
507 Laodica	105	-28	294	-25	4.70658	CE	323	4.71	3	45.2	115	-40	309	-30
508 Princetonia	132	41	313	13	52.676	CE	302	52.80	3	117.2	119	26	304	8
509 Iolanda	103	42			12.2907	CE	321	12.31	3	55.2	90	24	248	54
511 Davida	100	26	299	24	5.12937	E	344	5.13	3	270.3	299	24		5.12936

Table A.3. continued.

Asteroid	$\lambda_1$ [deg]	$\beta_1$ [deg]	$\lambda_2$ [deg]	$\beta_2$ [deg]	$P$ [hours]	M	$N_A$	$P_{LCDB}$ [hours]	D [km]	$\lambda_D$ [deg]	$\beta_{D1}$ [deg]	$\lambda_{D2}$ [deg]	$\beta_{D2}$ [deg]	$P_D$ [hours]	
512 Taurinensis	138	32	327	30	5.58203	CE	274	5.58	3	20.9	324	45	254	22	5.58203
516 Amherstia	255	24	7.4843	CE	341	7.48	3	65.1	81	54	286	-13	7.4843	22	
519 Sylvania	107	6	291	-10	17.9642	C	258	17.96	3	40.1	106	9	286	-13	17.9647
523 Ada	45	-64	253	-81	10.0324	CE	346	10.03	3	36.5	152	-70	357	-70	10.0324
528 Rezia	50	-56	179	-17	25.939	C	314	7.34	3	92.0	176	-59	46	-66	7.3380
529 Preziosa	6	-30	290	12	9.4049	C	287	27.00	2	41.2	2	-25	178	-10	25.939
532 Herculina	102	13	254	49	9.4689	CE	358	9.38	3	167.8	103	11	11	9.4049	9.4689
534 Nassovia	65	50	254	49	9.4689	CE	358	9.38	3	32.3	66	41	252	42	9.4689
536 Merapi	10	39	231	60	8.7904	CE	352	8.78	3	147.1	2	31	31	32	8.7905
537 Pauly	37	38	219	57	16.2957	CE	311	16.17	3	40.7	31	32	211	51	16.2961
543 Charlotte	171	40	336	61	10.7185	CE	239	10.72	3	45.6	333	59	172	49	10.7184
545 Messalina	154	47	306	41	7.4013	CE	317	7.20	3	112.6	312	47	156	46	7.4013
556 Phyllis	32	51	210	38	4.29262	CE	322	4.29	3	36.3	209	41	34	54	4.29262
558 Carmen	73	16	255	33	11.3901	C	330	11.39	3	54.8	254	-17	77	-35	11.3932
562 Salome	69	40			6.35044	C	325	6.35	3-	33.2	268	44	54	56	6.35032
563 Suleika	249	-46			5.63004	CE	311	5.69	3	52.2	251	-48			5.62998
564 Dudu	99	-38	238	-58	8.8851	CE	264	8.88	3	52.0	73	-51	213	-36	8.8850
565 Marbachia	175	-50	342	-26	4.58782	CE	216	4.59	3	27.8	163	-47	334	-22	4.58782
567 Eleutheria	131	58	315	41	7.7174	CE	288	7.72	3	88.7	317	33	131	53	7.7174
568 Cheruska	107	-49	293	36	13.2126	C	332	13.21	3	85.2	141	-2			13.2087
572 Rebekka	153	34	356	59	5.65008	CE	264	5.65	3	26.2	1	54	158	39	5.65009
573 Recha	80	-21	264	-46	7.16586	CE	240	7.17	3	47.6	76	-26			7.16585
579 Sidonia	265	-35			16.2870	E	344	16.29	3-	82.7	90	23			16.2804
582 Olympia	122	3	326	46	36.363	C	298	36.31	3	44.4	135	3			36.363
583 Klotide	316	58			9.2136	CE	297	9.21	3	84.5	150	40	327	54	9.2136
584 Semiramis	71	-71			5.06892	CE	367	5.07	3	48.7	75	-69			5.06893
586 Thekla	49	47	225	50	13.6815	CE	339	13.67	3	78.3	232	36	55	32	13.6816
588 Achilles	157	-6	337	9	7.30628	CE	212	7.31	3	133.2	172	-5			7.30630
589 Croatia	226	-43	368	-56	24.938	CE	305	24.82	2+	97.5	220	-39	35	-56	24.939
590 Tomyris	268	-45			5.55245	CE	355	5.56	3	30.6	274	-30	113	-35	5.55248
591 Irmgard	105	39	277	17	7.3451	CE	254	7.35	3	49.0	94	48	272	17	7.3451
593 Titania	7	39	212	73	9.8976	CE	347	9.90	3	77.2	175	58			9.8978
594 Mireille	118	-86			4.96893	E	136	4.97	3	9.2	208	-79			4.96929
595 Polyxena	46	8	227	-6	11.7942	CE	296	11.80	3	90.7	42	8	222	-4	11.7942
596 Scheila	110	-24	273	-38	15.8605	E	291	15.85	3	110.4	264	-18	89	-9	15.8666
597 Bandusia	171	1	356	-23	7.6648	C	272	7.66	3	40.6	355	-20	166	2	7.6644
598 Octavia	47	-19	224	0	10.8910	CE	278	10.89	3	78.1	222	-8			10.8912
600 Musa	36	-58	238	-27	5.88638	CE	299	5.89	3	25.1	208	-46	360	-74	5.88638
601 Nerthus	28	23	188	35	13.5898	C	326	13.59	3	75.5	173	44	20	32	13.5899
603 Timandra	154	75	313	67	330.3	E	174	41.79	3-	14.3	223	72			330.2
604 Tekmessia	5	89	203	87	5.55926	CE	318	5.56	3	64.5	158	74	305	62	5.55926
605 Juvisia	92	47	264	16	15.8429	C	305	15.93	2	62.7	90	28	269	-17	15.8418
606 Brangane	11	29	201	20	12.2907	CE	307	12.29	3-	35.8	183	20	354	26	12.2907

Table A.3. continued.

Asteroid	$\lambda_1$ [deg]	$\beta_1$ [deg]	$\lambda_2$ [deg]	$\beta_2$ [deg]	$P$ [hours]	M	$N_A$	$P_{LCDB}$ [hours]	D [km]	$\lambda_D$ [deg]	$\beta_{D1}$ [deg]	$\lambda_{D2}$ [deg]	$\beta_{D2}$ [deg]	$P_D$ [hours]	
614 Pia	4	60	168	44	4.57872	CE	207	4.57	3	29.2	162	27	348	48	4.57872
620 Drakonia	199	64	339	65	5.48713	CE	271	5.49	3	11.4	316	47	138	56	5.48711
622 Esther	128	-77	241	-59	47.504	CE	219	47.50	2	21.9	248	-60			47.504
624 Hektor	132	-13	328	-33	6.92047	CE	354	6.92	3	231.0	333	-31			6.92051
629 Bernardina	32	27	220	44	3.76359	CE	304	3.76	3	37.2	40	33	236	48	3.76360
630 Euphemia	8	71	194	85	387.0	E	302	350.00	2	15.5	2	54	125	71	387.0
631 Philippina	184	-3			5.90221	CE	269	5.90	3	50.5	183	-2			5.90220
635 Vundtia	104	50	296	69	11.7875	C	311	11.79	3	94.4	280	42	95	24	11.7873
636 Erika	14	-65	153	-64	14.6075	CE	328	14.60	3	76.1	13	-70	176	-60	14.6077
638 Moira	140	15	322	4	9.8751	C	283	9.88	3	59.6	327	10	144	22	9.8748
639 Latona	26	13	207	-10	6.19130	CE	325	6.19	3	78.5	25	12	204	10	6.19127
647 Adelgunde	68	-89	238	-72	98.10	CE	252	32.20	3	9.7	39	-68	252	-67	98.10
648 Pippa	79	-17	267	-31	9.2632	CE	300	9.26	3	76.0	69	-29	262	-39	9.2633
656 Beagle	100	81			7.03314	CE	315	7.04	3	62.6	237	86			7.03310
657 Gunlod	100	52	258	46	15.9287	C	251	15.67	3	39.4	267	33	104	44	15.9286
660 Crescentia	58	-67			7.9120	E	358	7.91	3	42.3	236	49	68	11	7.9104
662 Newtonia	161	-61	325	-66	21.1063	CE	335	21.09	3-	22.1	324	-43	126	-56	21.1062
665 Sabine	52	-54	307	-81	4.29404	CE	228	4.29	3	53.0	310	-77			4.29403
667 Denise	36	-81	235	-15	12.6845	E	340	12.69	3	88.6	40	-86			12.6848
669 Kypria	32	36	187	48	14.2787	CE	297	14.28	3	29.2	31	40	189	49	14.2789
670 Ottegebe	43	71	208	72	10.0399	CE	313	10.04	3	35.9	128	75			10.0399
674 Rachelle	35	-50	193	-30	30.976	CE	334	30.98	3	96.2	187	-36			30.975
675 Ludmilla	46	71			7.7155	CE	315	7.72	3	67.7	49	74	196	49	7.7155
679 Pax	41	-16	224	32	8.4559	C	250	8.45	3	63.9	42	-5	220	32	8.4560
682 Hagar	12	-56	227	-42	4.85043	C	165	4.85	3	255	-57	56	-78		4.85042
686 Gersuind	102	60			6.31238	CE	241	6.31	3	48.7	260	58	125	53	6.31240
689 Zita	188	-65	346	-62	6.42390	CE	196	6.42	3	15.6	256	-61	8	-72	6.42391
692 Hippodamia	222	-62			8.9969	C	308	8.98	3	42.8	233	-53			8.9969
694 Ekard	264	53			5.92194	CE	305	5.92	3	92.1	266	51			5.92193
695 Bella	314	-56			14.2189	CE	378	14.22	3	40.6	87	-55	314	-56	14.2190
698 Ernestina	83	-54	213	-64	5.03658	CE	251	5.04	3	26.7	213	-66	76	-49	5.03660
700 Auravictrix	68	49	267	55	6.07484	C	331	6.08	3	16.4	249	47	54	33	6.07488
706 Hirundo	53	79	211	84	22.0162	CE	236	22.03	3	29.4	92	66	244	54	22.0160
708 Raphaela	41	20	223	14	20.8897	CE	322	20.92	3-	21.0	37	27	217	22	20.8894
714 Ulula	227	-15			6.99837	CE	288	7.00	3	44.3	42	-9	227	-14	6.99838
718 Erida	92	-60	243	-69	17.4462	CE	313	17.45	3	70.9	257	-52	78	-56	17.4462
720 Bohlinia	46	42	230	40	8.9186	CE	258	8.92	3	34.2	239	40	33	52	8.9186
721 Tabora	179	49	346	29	7.9813	C	288	7.98	3	86.3	343	38	172	53	7.9812
731 Sorga	79	46	272	28	8.1863	C	326	8.18	3	34.6	274	21	83	42	8.1863
732 Tjilaki	7	71	349	55	12.3410	CE	285	12.34	3-	36.5	160	23	353	24	12.3411
733 Mocia	178	50			11.3761	CE	309	11.37	3	98.5	191	58			11.3762
734 Benda	92	52	272	35	7.10550	CE	283	7.11	3	67.3	272	50	101	53	7.10560
742 Edisona	22	-67	186	-40	18.5829	CE	332	18.52	3	47.1	9	-64	170	-39	18.5833

Table A.3. continued.

Asteroid	$\lambda_1$ [deg]	$\beta_1$ [deg]	$\lambda_2$ [deg]	$\beta_2$ [deg]	$P$ [hours]	M	$N_A$	$P_{LCDB}$ [hours]	D [km]	$\lambda_D$ [deg]	$\beta_{D1}$ [deg]	$\lambda_{D2}$ [deg]	$\beta_{D2}$ [deg]	$P_D$ [hours]
747 Winchester	177	-32	329	-46	9.4147	CE	271	9.41	3	170.1	304	-60	46	9.4148
749 Malzovia	62	50	252	58	5.92746	CE	265	5.93	3-	11.1	246	55	55	5.92748
752 Sulamitis	77	-43	245	-38	27.383	CE	268	27.37	3	60.2	248	-34	77	-36
753 Tiflis	210	70	334	-37	11.7372	C	238	9.85	3	26.5	5	36	199	57
754 Malabar	199	-37	334	-37	11.7372	C	379	11.74	3	91.3	334	-38	77	57
756 Lilliana	43	34	193	30	7.8325	CE	375	7.83	3	64.8	53	36	201	31
757 Portlandia	99	-39	272	-59	6.58108	CE	312	6.58	3	32.9	263	-69	90	-56
758 Mancunia	106	42	42	44	12.7200	CE	334	12.73	3	89.0	303	-40	114	52
760 Massinga	166	32	324	48	10.7611	E	382	10.72	3	70.0	156	47	10.7609	
769 Tatjana	204	86	312	62	35.064	CE	340	35.08	3-	96.7	347	38	176	54
770 Bali	65	44	257	44	5.81892	CE	301	5.82	3	16.4	70	50	262	45
771 Libera	64	-69	288	-29	5.89046	CE	275	5.89	3	28.2	64	-78	-78	-7
774 Armor	79	-18	263	-15	25.155	CE	395	25.11	2	50.2	261	-10	78	-7
784 Pickeringia	97	54	284	29	13.1700	CE	303	13.14	2+	75.6	103	68	282	35
785 Zwetana	266	62	62	8867	CE	280	8.89	3	50.7	270	61	278	20	8.8867
787 Moskva	332	54	54	6.05581	CE	274	6.06	3	32.0	331	59	126	27	6.05581
789 Lena	90	42	263	47	5.84235	CE	200	5.85	3	22.5	192	39	39	5.84239
791 Ani	93	-28	264	-3	11.1696	CE	321	11.17	3	99.8	94	-25	269	4
796 Sarita	21	65	65	8.1742	C	226	8.18	3	43.6	69	64	278	20	8.1743
797 Montana	14	60	180	47	4.54619	CE	304	4.55	3	21.2	6	61	179	45
798 Ruth	88	9	260	36	8.5508	C	339	8.55	3	45.2	84	27	8.5507	
799 Gudula	131	75	342	70	14.8108	C	356	14.81	3	47.2	350	46	159	45
800 Kressmannia	156	59	323	60	4.46094	C	246	4.46	3	15.4	345	37	172	34
802 Epyaxa	94	-55	225	29	4.39012	C	153	4.39	3	7.4	347	-87	-87	4.39012
803 Picka	55	36	225	29	5.07479	CE	240	5.07	3	57.4	53	41	218	34
804 Hispania	87	-18	264	-49	14.8476	CE	300	14.85	3	149.7	90	2	268	-35
807 Ceraskia	133	18	324	26	7.3738	C	255	7.37	3	21.2	132	26	325	23
808 Merxia	25	62	183	62	30.630	CE	387	30.63	3	30.9	26	54	192	57
820 Adriana	100	19	285	22	12.4064	E	278	6.53	2	63.8	284	29	98	24
823 Sisigambis	176	46	353	63	146.57	CE	247	146.00	2	14.7	186	48	48	146.58
824 Anastasia	144	73	342	72	252.0	CE	225	250.00	3-	32.5	289	86	56	62
829 Academia	45	-53	192	-69	7.8933	CE	226	7.89	3-	41.2	245	-67	71	-41
830 Petropolitana	237	48	334	20	14.8249	CE	315	14.83	3	24.9	242	46	59	44
832 Karin	60	48	237	50	18.3513	CE	212	18.35	3	15.8	242	341	18	14.8247
842 Kerstin	62	53	256	11	18.7146	C	223	18.72	2	43.6	261	34	57	66
844 Leontina	185	48	336	54	6.78301	CE	356	6.79	3	42.1	302	68	31	34
847 Agnia	155	12	334	20	14.8249	CE	315	14.83	3	24.9	341	18	162	13
849 Ara	221	-36	47	44	9.3317	CE	286	4.12	3	80.8	223	-41	-41	4.11639
851 Zetissia	108	47	291	44	3.00367	CE	270	9.34	3	12.6	275	68	62	9.3316
855 Newcoombia	147	-26	346	-43	8.2075	CE	215	3.00	3	12.4	357	-87	-87	3.00368
857 Glasenappia	37	38	28	9.3023	CE	271	8.20	3	14.5	38	34	227	48	8.2076
860 Ursina	68	55	331	52	11.0566	CE	299	10.95	3	34.6	73	60	11.0566	
861 Aida	170	72	331	52	11.0566	CE	299	10.95	3	69.6	294	70	70	11.0566

Table A.3. continued.

Asteroid	$\lambda_1$ [deg]	$\beta_1$ [deg]	$\lambda_2$ [deg]	$\beta_2$ [deg]	P [hours]	M	$N_A$	$P_{LCDB}$ [hours]	D [km]	$\lambda_D$ [deg]	$\beta_{D1}$ [deg]	$\lambda_{D2}$ [deg]	$\beta_{D2}$ [deg]	$P_D$ [hours]	
868 Lova	31	-39	210	-28	41.152	CE	276	41.12	3	50.7	41	-49	217	-28	41.151
870 Manto	93	25	279	24	122.18	CE	230	122.30	3	11.9	95	31	288	33	122.17
872 Holda	80	25	5.94052	CE	310	5.95	3	34.4	253	32	77	24	5.94052		
874 Rotrat	211	-51	358	-52	14.3008	C	339	14.30	3-	58.3	2	-36	201	-41	14.3007
877 Walkure	48	68	234	74	17.4218	CE	301	17.42	3-	39.9	47	66	262	71	17.4217
881 Athene	2	-34	180	-78	13.8945	CE	187	13.89	3-	12.2	115	-77	338	-43	13.8943
888 Parysatis	102	-64	254	-41	5.93336	C	302	5.93	3	44.8	263	-47	127	-62	5.93333
889 Erynia	14	-62	201	-44	9.8748	CE	190	9.89	3	16.7	187	-60	335	-74	9.8749
890 Waltraut	9	46	177	53	12.5831	CE	195	12.58	3	28.4	122	72	30	69	12.5831
893 Leopoldina	173	-16	340	-28	12.5991	C	311	14.12	3	76.6	331	-42	179	-17	12.5993
899 Jokaste	174	-104	349	-62	6.24812	CE	281	6.25	3	31.0	71	-50	50	6.24811	
905 Universitas	89	-50	256	-52	14.2420	CE	249	14.24	3	10.6	113	-57	276	-60	14.2420
908 Buda	44	4	230	22	14.5744	C	306	14.57	3	30.7	40	5	225	16	14.5750
915 Cosette	7	46	199	53	4.46975	CE	280	4.45	3	11.7	189	61	350	56	4.46974
918 Itha	236	-74	219	50	3.47380	CE	202	3.47	3	20.3	72	-54	214	37	3.47381
924 Toni	44	27	19	50	19.4374	C	286	19.44	3	78.3	40	32	214	37	19.4373
925 Alphonsina	285	48	7.8775	C	327	7.88	3	57.5	294	41	41	41	7.8775		
934 Thuringia	120	-64	8.1653	CE	178	8.17	3	53.7	120	-52	120	-52	8.1653		
940 Kordula	82	-46	15.5641	CE	339	15.57	3	79.8	272	-39	102	-30	102	-30	15.5639
950 Ahrensa	86	18	132	61	205.7	CE	286	202.00	3	13.7	10	89	89	89	205.7
952 Caia	64	19	247	13	7.5011	CE	303	7.51	2	88.7	239	-19	19	-19	7.5010
955 Alstede	51	67	244	34	5.18734	CE	292	5.19	3	17.2	64	57	246	23	5.18734
956 Elisa	66	-40	255	-46	16.4987	E	212	16.49	3	10.5	67	-46	252	-33	16.4984
968 Petunia	38	-59	252	-45	61.159	CE	291	61.28	3	24.4	355	-78	78	-78	61.160
976 Benjamina	160	54	343	68	9.7082	E	291	9.70	3	83.2	151	40	336	60	9.7083
977 Philippa	132	-63	221	-71	15.4042	CE	303	15.40	3	65.5	213	-67	85	-66	15.4043
984 Gretia	239	43	5.77801	CE	258	5.78	3	32.5	245	52	52	52	52	52	5.77803
986 Amelia	85	30	9.5187	CE	299	9.52	3	48.7	282	30	80	30	80	30	9.5185
993 Moultona	176	-69	326	-68	5.27012	CE	214	5.27	3	15.2	22	40	199	34	5.27004
999 Zachia	28	38	191	34	22.836	CE	257	22.84	3	16.9	28	29	199	24	22.836
1002 Olbersia	22	59	220	36	10.2367	CE	238	10.24	3	22.9	220	35	16	54	10.2367
1010 Marlene	95	37	284	37	31.065	CE	289	31.06	2+	46.9	106	47	299	42	31.065
1012 Sarena	51	45	242	50	10.3071	CE	128	10.32	3	20.9	51	64	254	53	10.3071
1013 Tombecka	17	48	235	51	6.05015	CE	265	6.05	3	34.6	244	34	54	46	6.05018
1021 Flammario	0	104	184	74	12.1519	CE	310	12.16	3-	100.8	216	55	32	22	12.1518
1022 Olympiada	44	25	262	34	9.0821	E	262	9.08	3	56.1	247	29	31	69	9.0822
1029 La Plata	91	47	276	39	15.3106	CE	225	15.31	3	16.5	293	56	241	67	3.83359
1032 Pafuri	136	83	338	56	112.80	CE	280	33.39	3-	65.7	178	67	355	47	112.81
1035 Amata	45	81	262	34	3.83359	CE	302	3.82	3	32.9	39	17	241	67	3.83359
1040 Klumpke	339	-29	37.733	E	175	59.20	2	22.3	172	48	48	48	48	56.588	
1054 Forsytia	183	70	357	42	7.6497	CE	321	7.65	3	53.0	187	61	61	76.498	
1056 Azalea	54	34	243	46	15.0275	CE	261	11.89	2+	11.9	252	51	64	41	15.0276
1069 Planckia	50	44	215	73	8.6584	CE	322	8.66	3	35.7	197	83	8.6585		

Table A.3. continued.

Asteroid	$\lambda_1$ [deg]	$\beta_1$ [deg]	$\lambda_2$ [deg]	$\beta_2$ [deg]	$P$ [hours]	M	$N_A$	$P_{LCDB}$ [hours]	D [km]	$\lambda_D$ [deg]	$\beta_{D1}$ [deg]	$\lambda_{D2}$ [deg]	$\beta_{D2}$ [deg]	$P_D$ [hours]
1075 Helina	125	-43	44.677	CE	251	44.90	3-	37.9	128	-43	281	-45	44.677	
1082 Pirola	125	-69	296	-65	15.8543	CE	244	15.85	3	48.4	123	-42	300	-38
1083 Salvia	96	-53	267	-59	4.28144	CE	197	4.23	3	8.9	358	-58	165	-59
1085 Amaryllis	175	-61	331	-67	18.1425	E	345	18.11	3-	69.3	325	-75	184	-64
1088 Mitaka	112	-38	281	-54	3.03537	CE	278	3.04	3	15.1	280	-71		3.03538
1102 Pepita	27	-48	242	-43	5.10532	CE	370	5.11	3	36.6	25	-34	231	-30
1107 Lictoria	68	62	294	65	8.5611	CE	334	8.56	3	79.1	282	64	96	52
1110 Jaroslawia	101	67	322	62	97.27	CE	307	97.40	3-	12.3	236	75		97.28
1116 Catronia	114	51	282	20	8.8360	C	176	8.83	3	38.7	292	18		8.8360
1118 Hanskya	72	-44	299	-77	25.308	E	254	15.61	2	71.0	72	-52	344	-82
1119 Euboea	45	55	254	58	11.3979	CE	197	11.41	3	29.4	282	55	79	75
1126 Otero	58	89	285	62	3.64800	CE	209	3.65	3	12.0	44	75	240	56
1127 Mimi	274	-76	213	-53	12.7456	CE	290	12.75	3	46.0	224	-57		12.7456
1135 Colchis	48	-45	213	-53	23.482	CE	262	23.47	2	50.6	139	-58	330	-81
1137 Raissa	158	-76	330	-91	143.65	CE	215	142.79	3-	19.4	220	-66	40	-77
1140 Crimea	53	-73	126	-36	9.7870	E	208	9.77	3	28.5	112	-73	175	-22
1148 Rarahu	147	-7	324	-7	6.54448	CE	327	6.54	3-	27.5	146	-3	327	-2
1157 Arabia	50	-51	160	-84	11.5472	CE	271	15.22	3-	29.0	43	-52	205	-61
1160 Illyria	68	78	269	50	4.10296	CE	250	4.10	3	14.0	87	65		4.10295
1186 Turnera	205	50	12.0851	CE	329	12.09	3	34.3	206	63				12.0851
1188 Gothlandia	57	-72	3.49182	CE	272	3.49	3	12.2	334	-84				3.49182
1189 Terentia	102	-63	321	-54	19.3090	CE	268	19.31	3	59.2	50	-52		19.3090
1196 Sheba	96	64	6.31379	CE	322	6.32	3	33.2	113	72				6.31376
1200 Imperatrix	128	39	308	58	17.7783	CE	247	17.77	3	42.0	343	68	182	51
1202 Marina	65	-30	241	-36	9.4580	C	217	9.45	3	63.8	228	-43	54	-47
1207 Osteria	130	-64	372	-72	9.0713	CE	237	9.07	3	22.9	51	-60	183	-63
1214 Richilde	118	-54	326	-43	9.8667	CE	245	9.86	3	36.7	59	-64	275	-46
1223 Neckar	72	34	255	33	7.8239	CE	311	7.81	3	22.8	69	30	252	28
1228 Scabiosa	65	-68	259	-73	22.697	E	220			16.2	122	-86		22.697
1237 Genevieve	83	-48	228	-63	24.715	E	368	16.37	2	43.0	246	5	64	8
1241 Dysona	33	-25	112	-74	8.6074	CE	408	8.61	3-	79.2	124	-68	20	-23
1245 Calvinia	54	-47	236	-42	4.85147	CE	283	4.85	3	29.8	52	-51	235	-43
1248 Jugurtha	63	-86	12.1904	CE	335	12.91	3	28.5	74	-89				12.1905
1251 Hedera	23	-62	192	-63	19.9020	CE	229	19.90	3-	13.2	271	-53	115	-63
1256 Normannia	78	-18	261	-12	489.7	CE	236	488.06	2	73.3	84	-25		489.8
1263 Varsavia	335	-13			7.1650	CE	320	7.16	3	51.4	341	-14		7.1650
1275 Cimbria	91	-58	274	-26	5.65456	CE	323	5.65	3	27.6	271	-31	85	-61
1276 Ucilia	106	-54	247	-16	4.90747	CE	190	4.91	3	36.5	154	-69		4.90747
1283 Komsomolia	69	40	248	67	32.196	CE	248	32.17	3	29.6	76	31	261	48
1284 Latvia	85	-22	282	-46	9.5538	CE	272	9.55	3-	41.1	105	32		9.5506
1291 Phryne	111	42	271	68	5.58413	CE	241	5.58	3	27.4	109	34	281	56
1299 Mertonia	85	41	271	50	4.97692	CE	151	4.98	3	14.2	73	35	253	56
1301 Yvonne	53	29			7.3197	CE	252	7.32	3	21.4	39	41		7.3197

Table A.3. continued.

Asteroid	$\lambda_1$ [deg]	$\beta_1$ [deg]	$\lambda_2$ [deg]	$\beta_2$ [deg]	P [hours]	M	$N_A$	$P_{LCDB}$ [hours]	D [km]	$\lambda_D$ [deg]	$\beta_{D1}$ [deg]	$\lambda_{D2}$ [deg]	$\beta_{D2}$ [deg]	$P_D$ [hours]
1312 Vassar	108	-50	256	-13	7.9319	CE	251	7.93	3	32.7	251	-23		7.9319
1317 Silvretta	42	-49	152	-54	7.0679	CE	268	7.05	3	26.4	161	-46	45	-57
1332 Marconia	54	50	239	52	32.120	E	283	19.16	3	46.8	240	26	59	26
1333 Cevenola	16	-81	210	-43	4.87933	CE	225	4.88	3	15.3	38	-86	220	-44
1335 Demoulina	84	56	278	61	74.94	CE	104	74.86	2+	7.5	31.8	58	126	60
1349 Bechuana	156	31	322	38	15.6878	CE	306	15.69	3-	24.2	31.4	46	153	32
1350 Rosselia	72	-72	246	-60	8.1401	CE	223	8.14	3	20.8	67	-64	246	-58
1351 Uzbekistania	54	-60	194	-62	73.98	CE	330	73.90	2	60.0	41	-58		73.98
1353 Maartje	107	49	279	70	22.9925	CE	269	22.93	3	39.0	285	74	120	42
1366 Piccolo	187	47	348	43	16.1834	CE	345	16.57	2	26.9	352	49	201	55
1378 Leonce	10	-73	206	-88	4.32526	CE	200	4.33	3	21.2	46	-77	210	-67
1379 Lomonosowa	272	-47	24.485	CE	289	24.49	3	18.7	72	-84	265	-46		24.485
1389 Onnie	131	-93	264	-74	23.0449	CE	197	22.50	2	13.8	183	-75	360	-79
1390 Abastumani	144	18	327	-21	13.1646	CE	323	17.10	2	95.8	148	25		13.1648
1396 Outerinqua	69	74	259	73	3.08174	CE	255	3.08	3	11.7	242	61	55	3.08175
1398 Donnera	2	39	188	15	7.2315	CE	293	7.23	3	28.3	1	44		7.2316
1400 Tirela	104	-66	291	-28	13.3540	CE	122	13.36	2	15.7	58	-80	297	-41
1403 Idelsonia	147	-15	322	-6	5.45928	CE	179	5.46	3	26.5	325	9	141	4
1413 Roucarie	120	26	311	46	6.53059	CE	222	6.36	3	19.8	310	33	124	15
1423 Jose	81	-64	256	-72	12.3127	CE	270	12.31	3	19.6	78	-82		12.3127
1431 Luanda	206	-72	273	-75	4.13594	CE	223	4.14	3-	13.6	18	-87		13.3538
1434 Margot	199	-49	351	-73	8.2281	CE	313	8.17	3	27.2	348	-62	196	-47
1436 Salonta	56	38	219	28	8.8698	CE	315	8.87	3	53.8	223	18	57	35
1459 Magnya	41	-102	141	-63	4.67910	CE	226	4.68	3	29.9	207	-51	72	-59
1461 Jean-Jacques	169	-17	329	-58	16.5610	C	258	16.56	2	35.1	149	-12	319	-23
1484 Postrema	19	36	12.1897	CE	223	12.19	3-	40.9	19	44	250	19	250	64
1490 Limpopo	150	22	318	51	6.65158	CE	181	6.65	3	14.8	142	2	319	22
1493 Sigrid	117	79	43.179	CE	224	43.30	2	28.9	350	69	183	69	43.179	
1500 Jyvaskyla	101	-66	255	-78	8.8275	CE	142	8.83	2	8.1	268	-79	123	-75
1503 Kuopio	43	-71	71	9.9586	CE	320	9.96	3	22.3	27	-61	170	-86	
1542 Schaeen	82	37	260	38	7.5154	C	276	7.52	3	42.4	259	53	82	53
1545 Thermo	142	-55	316	-62	17.2031	CE	175	17.20	3	17.3	352	-80	164	-75
1547 Nele	311	53	7.0974	CE	268	7.10	3	16.8	318	50	159	28	7.0974	
1554 Yugoslavia	43	-69	280	-41	3.88768	CE	177	3.89	3	16.2	281	-34	78	-64
1568 Aisien	112	-67	667605	C	208	6.68	3	11.6	109	-68			6.67597	
1572 Posmania	81	-61	226	-78	8.0493	CE	231	8.05	3	27.8	205	-82	85	-63
1584 Fujii	107	20	286	-18	14.8872	CE	286	14.88	3	16.7	104	22		14.8865
1590 Tsiolkovskaja	98	6	277	16	6.72899	C	222	6.73	3	10.3	277	12	99	-6
1591 Baize	20	-14	192	46	7.7935	E	215	7.79	3-	14.4	189	45	5	-2
1609 Brenda	19	52	199	-47	19.7699	C	301	19.78	3	28.0	200	-52		19.7856
1621 Druzhba	157	86	348	98	99.10	CE	211	99.20	3	11.7	240	71		99.10
1633 Chimay	88	76	286	72	6.59059	CE	237	6.59	3	37.4	116	81	322	77
1635 Bohrmann	5	-35	188	-33	5.86427	C	271	5.86	3	17.1	5	-38	185	-36

Table A.3. continued.

Asteroid	$\lambda_1$ [deg]	$\beta_1$ [deg]	$\lambda_2$ [deg]	$\beta_2$ [deg]	$P$ [hours]	M	$N_A$	$P_{LCDB}$ [hours]	D [km]	$\lambda_D$ [deg]	$\beta_{D1}$ [deg]	$\lambda_{D2}$ [deg]	$\beta_{D2}$ [deg]	$P_D$ [hours]	
1636 Porter	87	15	267	25	2.96594	E	178	2.97	3	8.4	265	65	85	52	2.96559
1637 Swings	46	58	255	38	10.2695	E	291	10.26	3	53.0	232	26	43	37	10.2695
1643 Brown	117	62	282	58	5.93124	C	187	5.93	3	9.5	140	64	353	84	5.93124
1645 Waterfield	138	-24	318	-23	4.84434	E	234	4.86	3	28.1	151	59	336	43	4.84349
1659 Punkaharju	82	-35	276	-69	5.01329	CE	272	5.01	3	28.2	259	-71	75	-22	5.01327
1663 van den Bos	256	69	351	66	748.7	CE	184	740.00	3-	10.8	249	62	43	52	748.7
1677 Tycho	9	-60	110	-64	3.85667	CE	164	3.85	3-	11.8	35	-61			3.85665
1691 Oort	87	58	266	58	10.2685	CE	217	10.27	3	33.6	223	58	45	68	10.2684
1693 Hertzsprung	265	65			8.8422	E	215	8.82	3	37.8	45	47	255	48	8.8423
1709 Ukraina	152	-42	336	-28	7.3052	E	132	7.28	3	10.8	165	-61	2	-40	7.3052
1715 Salli	96	-42	258	-48	11.0890	CE	154	11.09	3	23.1	95	-24	254	-48	11.0887
1723 Klemola	254	-60	60		6.25609	CE	294	6.25	3	33.5	80	-59	253	-36	6.25610
1727 Mette	300	-62			2.98120	CE	249	2.98	3	6.1	307	-62			2.98117
1728 Goethe	40	-74	288	-68	120.97	CE	239	81.00	2	18.2	267	-76	42	-73	120.98
1730 Marceline	70	56	271	68	3.83655	CE	122	3.84	3	15.2	82	44	264	68	3.83654
1735 ITA	29	-44	177	-38	12.6105	CE	278	12.60	3-	66.1	39	-46	178	-52	12.6103
1742 Schaffers	12	67	175	64	8.5327	CE	237	8.56	3	16.7	198	57	46	55	8.5327
1789 Dobrovolsky	145	17	326	17	4.81106	CE	154	4.81	3	7.9	137	34	319	30	4.81110
1794 Finsen	71	78	165	54	12.3462	CE	187	12.35	2	38.0	3	65	169	35	12.3465
1804 Chebotarev	66	66	247	58	4.02373	C	190	4.03	3	9.2	188	54	4	59	4.02375
1816 Liberia	137	-82	199	-46	3.08615	CE	224	3.09	3	12.5	73	-68			3.08616
1825 Klare	17	-54	196	-67	4.74290	CE	163	4.74	3	14.7	2	-58			4.74288
1847 Stobbe	163	-58	336	-73	5.61755	C	335	5.62	3	17.4	356	-82			5.61757
1848 Delvaux	135	-73	325	-75	3.63910	CE	128	3.64	3	17.0	86	-58	269	-62	3.63911
1860 Barbarossa	56	38	241	58	3.25486	CE	252	3.25	3	16.8	238	63	45	30	3.25485
1888 Zu Chong-Zhi	175	41	358	52	11.0511	C	157	11.05	3	11.6	338	49			11.0512
1927 Suvanto	271	7	274	15	8.1613	C	134	8.16	3	11.8	278	23	74	73	8.1615
1946 Walraven	44	-60	180	-63	10.2101	C	192	10.21	2+	9.2	259	-80	80	-59	10.2101
1958 Chandra	74	-64	258	-80	7.0570	CE	186	7.07	3-	34.3	152	-35	310	-43	7.0569
1980 Tezcatlipoca	290	-62	331	-12	7.2522	CE	180	7.25	3	6.0	324	-69			7.2523
1996 Adams	103	54	278	32	3.31115	E	249	3.31	3	12.4	107	55			3.31114
1999 Hirayama	172	-64	302	-70	15.6237	CE	261	15.63	3-	35.7	264	-34	89	-66	15.6239
2001 Einstein	87	-54	266	-125	5.48502	C	147	5.49	3	4.0	87	-43			5.48503
2013 Tucapel	58	-34	231	-12	9.0292	CE	181	9.03	3	11.2	69	-33	237	-33	9.0292
2043 Ortuiay	88	-77	270	-51	7.7476	CE	228	7.75	3-	48.5	305	-73	101	-62	7.7477
2064 Thomsen	75	-69	254	-87	4.24400	CE	132	4.23	3	8.1	118	-72	334	-56	4.24402
2091 Sampo	215	-26			71.129	CE	231	71.34	2	23.0	213	-24			71.140
2094 Magnitka	86	62	248	56	6.11218	C	224	6.11	3	10.1	107	57	272	48	6.11219
2104 Toronto	242	-64			8.9668	CE	337	8.97	3	35.9	241	-68			8.9668
2120 Tyumenia	92	34	235	51	17.4984	CE	209	17.51	2	42.3	244	45	92	23	17.4991
2185 Guangdong	99	-34	252	-63	21.077	E	242	21.09	3-	12.7	259	-46	96	-33	21.077
2216 Kerch	137	-57	291	-45	9.4660	E	206	9.46	3-	18.0	142	-60			9.4661
2235 Vittore	227	48			32.121	C	243	32.10	3	41.7	222				32.124

Table A.3. continued.

Asteroid	$\lambda_1$ [deg]	$\beta_1$ [deg]	$\lambda_2$ [deg]	$\beta_2$ [deg]	$P$ [hours]	M	$N_A$	$P_{LCDB}$ [hours]	D [km]	$\lambda_D$ [deg]	$\beta_{D1}$ [deg]	$\lambda_{D2}$ [deg]	$\beta_{D2}$ [deg]	$P_D$ [hours]	
2239 Paracelsus	283	58	6.09756	CE	204	6.10	3-	35.2	280	-30				6.09829	
2272 Montezuma	286	-47	8.1888	CE	96	8.18	3	5.3	108	0				8.1864	
2275 Cuithahuac	4	-40	6.29009	CE	181	6.29	3	7.0	9	-65				6.29005	
2292 Seili	137	71	5.12489	C	248	5.12	3	11.3	148	63				5.12487	
2309 Mr. Spock	63	-48	6.72086	C	224	6.72	3	19.7	255	-41	78	-55		6.72088	
2358 Bahner	8	66	10.8541	C	168	10.85	3	18.6	193	52	0	57		10.8529	
2397 Lappajarvi	80	-43	9.0532	C	212	9.04	3-	16.4	82	-54	255	-35		9.0532	
2420 Ciurlionis	80	-4	15.7285	CE	105	15.76	3-	8.4	267	17				15.7286	
2425 Shenzhen	81	74	9.8382	E	203	14.71	3	18.7	265	40	50	58		9.8382	
2448 Sholokhov	189	-15	10.0632	C	294	10.06	3	38.5	351	-49				10.0633	
2468 Repin	19	68	5.11905	C	102	5.12	3	6.2	183	57	25	58		5.11904	
2490 Bussolini	20	-68	261.7	CE	126	24.00	1	11.7	117	-81				261.8	
2566 Kirghizia	92	-39	4.44888	C	132	4.45	3	7.8	262	-55	91	-39		4.44887	
2590 Mourao	116	30	15.5745	CE	187	15.59	3	7.9	115	36	291	47		15.5745	
2606 Odessa	18	-53	8.2444	CE	179	8.24	3	15.9	283	-88	25	-81		8.2445	
2617 Jiangxi	13	49	11.7727	CE	239	11.77	3	49.1	239	76	359	56		11.7730	
2634 James	96	-50	16.5147	C	213	16.51	2	33.7	126	-46	292	-43		16.5146	
2649 Oongaq	127	38	7.7854	C	179	7.79	3	11.4	172	33	356	75		7.7854	
2677 Joan	13	-68	16.9788	CE	149	16.98	3	17.7	253	-35	53	-53		16.9787	
2706 Borovsky	111	68	303	46	63.80	C	94	63.85	2	15.0	317	67		63.79	
2715 Mielikki	20	55	179	50	33.599	CE	172	33.62	3-	13.2	1	75	65	33.598	
2725 David Bender	124	-72	233	26	9.9574	CE	249	9.96	3-	42.9	58	-57	198	-37	9.9580
2839 Annette	155	-39	340	-48	10.4609	CE	155	10.46	3	7.3	154	-36	341	-49	10.4609
2854 Rawson	36	-47	230	-70	4.77559	CE	158	4.78	3	7.2	336	-83		4.77559	
2889 Brno	40	56	199	44	9.5322	CE	116	9.51	2+	17.2	46	55		9.5320	
2957 Tatsuo	88	46	247	47	6.82041	CE	219	6.82	3	22.5	81	45	248	32	6.82042
2962 Otto	70	44			2.67805	C	241	2.68	3	15.1	230	-58			2.53632
2973 Paola	20	-57	196	-77	155.35	E	71	24.00	1	14.3	182	-79	41	-68	155.26
3017 Petrovic	187	-71	353	-65	4.08037	CE	241	4.08	3	12.8	9	-55			4.08036
3066 McFadden	113	-69	279	-21	32.752	C	328	13.80	3	13.5	132	-80			32.752
3169 Ostro	134	-29	241	-54	6.50917	CE	165	6.50	3	4.7	247	-56			6.50916
3210 Lupishko	38	57	269	98	14.2491	CE	217	14.26	2+	19.1	136	86			14.2492
3232 Brest	98	56	287	71	154.04	E	133	5.29	2	20.3	36	78	159	59	154.03
3266 Bernardus	230	-33			10.7596	C	195	10.76	3	6.2	227	-32			10.7595
3314 Beals	31	66	242	42	5.46136	C	100	5.46	3	6.8	159	-42	358	-46	5.46233
3332 Raksha	17	100			4.80563	CE	239	4.81	3	14.6	204	78			4.80563
3376 Armandhammer	145	-10	325	10	7.9110	CE	177	7.92	3-	7.9	316	11	136	-1	7.9112
3383 Koyama	84	47	282	79	111.76	CE	162	111.84	2	10.6	70	68			111.77
3613 Kunlun	304	82	347	57	308.9	CE	127				311	67	80	69	308.9
3623 Chaplin	15	-59	193	-53	8.3498	C	105	8.36	3	9.9	168	-50	345	-55	8.3498
3772 Piaf	64	54	260	62	5.37611	CE	208	5.38	3	19.0	136	63	336	67	5.37617
3776 Vartiovuori	119	-7	284	-65	11.3414	E	221	11.34	2	22.5	284	-64			111.3410
3786 Yamada	75	59	218	44	4.03295	CE	277	4.03	3	15.8	218	48	84	52	4.03295

Table A.3. continued.

Asteroid	$\lambda_1$ [deg]	$\beta_1$ [deg]	$\lambda_2$ [deg]	$\beta_2$ [deg]	$P$ [hours]	M	$N_A$	$P_{LCDB}$ [hours]	D [km]	$\lambda_D$ [deg]	$\beta_{D1}$ [deg]	$\lambda_{D2}$ [deg]	$\beta_{D2}$ [deg]	$P_D$ [hours]	
3811 Karma	89	51	263	19	14.4236	C	141	13.23	2+	30.3	89	52	264	12	14.4234
3883 Verban	238	-50	349	-74	50.919	CE	220	50.80	2+	11.8	206	-75	346	-63	50.921
3924 Birch	62	17	242	-2	18.6684	CE	94	18.74	2	16.8	238	17	57	37	18.6720
3935 Toatenmongakkai	165	-10	345	-2	103.90	E	104	106.30	2	9.6	294	-84	35	45	104.29
4012 Geballe	172	35	353	52	5.88574	E	97	5.89	3	5.8	145	35	326	45	5.88571
4077 Asuka	36	62	272	65	7.9231	CE	217	7.92	3-	19.5	267	44	57	45	7.9231
4088 Baggesen	18	75			6.45273	E	169			6.5	40	36	232	31	6.45277
4102 Gergana	108	47	290	68	5.22345	E	76			12.0	95	68			5.22340
4132 Bartok	266	87			3.29632	C	123			3.30	3	9.7	186	87	3.29633
4163 Saaremaa	70	37	263	56	26.327	E	154			19.9	264	60	89	28	26.327
4170 Semmelweis	111	51	315	80	5.30524	C	147			16.8	262	89			5.30526
4222 Nancita	41	-58	240	-48	3.87292	CE	129	3.87	3	9.6	45	-42	238	-40	3.87292
4271 Novosibirsk	97	43	302	68	8.8468	E	153	8.85	3	246	84				8.8468
4285 Hulkower	181	-44	249	-65	6.14987	E	93	6.15	3	7.8	235	-65			6.14986
4374 Tadamori	144	-68	290	-54	4.50495	C	107	4.50	3	5.7	190	-41	7	-54	4.50495
4483 Petoff	88	52			4.33363	E	127	4.33	3	5.8	107	40			4.33299
4611 Vulkaneifel	147	31	341	13	3.75596	E	124	3.76	3	11.0	197	-50	5	-86	3.75636
4800 -	111	-67	286	-44	6.21566	CE	109	6.22	2	14.1	274	16	94	-9	6.21486
4810 Ruslanova	343	68			69.76	E	72	69.76	2	6.3	124	55			69.76
4820 Fay	127	-82	344	-65	3.72739	C	108	3.73	3	8.6	248	-67	67	-40	3.72744
5111 Jacliff	98	-57	292	-34	2.83989	E	108	2.84	3	6.5	259	-45			2.83990
5247 Krylov	336	-48			82.29	CE	160	81.50	2	7.7	262	-42			82.29
5281 Lindstrom	35	-75	209	-52	9.2512	CE	154	9.25	2	17.0	84	-81	238	-72	9.2511
5488 Kiyosato	68	75	282	74	8.7632	CE	165	8.79	2	18.8	19	23	242	62	8.7631
5596 Morbidelli	22	-64	194	-70	5.3992	E	65	5.40	3	5.7	173	-80			5.4004
5647 -	185	54			6.13971	E	147	6.14	3	8.6	266	69			6.13867
5687 Yamamotohinobu	209	-71	306	-86	154.88	E	154			13.8	66	-89			154.87
5776 -	175	-66	333	-34	4.34076	E	65	4.34	2	360	-72				4.34079
5925 -	276	-32			5.39962	E	63	5.40	3	6.1	321	-63	128	-46	5.40076
5933 Kemurdzhian	24	-31	201	-34	4.75566	E	60			3.6	223	-62	40	-60	4.75651
6882 Sormano	113	-37	316	-37	3.99835	CE	108	3.69	2	8.1	43	-33	248	-58	3.99835
7151 -	58	-48	243	-33	5.07202	E	119	5.07	3	9.4	182	-52			5.07205
7233 Majella	40	-41			3.81244	E	110	3.81	3	80	-71	298	-87		3.81240
8380 Tooting	152	-30			36.892	E	90	36.93	3	10.0	248	33	85	17	36.894
8532 -	110	49	307	12	112.59	E	63	30.00	2	8.8	292	68			112.61
12008 Kandrup	19	-35			32.940	CE	141	32.90	3	4.2	351	-61			32.940
12690 -	48	-73	303	-46	147.34	E	132			15.3	282	-62	112	-87	147.35
16009 -	86	71	292	44	16.6910	CE	191	16.70	2+	10.1	283	44			8.3476
21652 Vasishta	346	-49			16.287	E	68	16.29	3	10.5	336	-45			16.288

**Notes.** We provide ecliptic coordinates  $\lambda$  and  $\beta$  of up to two pole solutions, sidereal rotational period  $P$  (its uncertainty is of the order of the last digit). The method (M) column indicates whether the rotation period was derived by the convex inversion (C), ellipsoid (E) approach, or both (CE) approaches. The final columns are the number of ASAS-SN measurements  $N_A$ , the LCDB period with its reliability flag (Warner et al. 2009), the size  $D$  from the MP3C database<sup>4</sup>, and the DAMIT rotation state solution.

**Table A.4.** Physical properties of asteroids with new rotation period determinations based on the *V*-band ASAS-SN data.

Asteroid	<i>P</i> [hours]	M	<i>N<sub>A</sub></i>	<i>D</i> [km]
835 Olivia	1104.0	C	145	30.4
991 McDonalda	339.5	E	178	38.6
1034 Mozartia	449.9	E	216	9.7
1445 Konkolya	59.395	C	96	20.3
1714 Sy	317.8	E	193	14.0
1745 Ferguson	1078.2	C	136	12.1
1755 Lorbach	7.9765	CE	208	24.9
1787 Chiny	13.5609	E	173	19.9
1984 Fedynskij	8.1405	E	187	38.4
2027 Shen Guo	1117.3	E	164	16.5
2051 Chang	12.0142	CE	183	16.4
2138 Swissair	369.7	C	244	12.9
2158 Tietjen	8.6581	E	137	22.7
2165 Young	6.39009	CE	143	27.1
2191 Uppsala	31.317	E	213	17.5
2219 Mannucci	27.460	E	172	39.1
2226 Cunitza	189.05	E	159	14.6
2248 Kanda	24.736	E	169	26.4
2404 Antarctica	2.26238	CE	143	23.2
2405 Welch	14.3411	E	123	26.4
2413 van de Hulst	211.96	E	190	20.8
2475 Semenov	12.2370	E	131	14.5
2502 Nummela	14.3151	E	97	19.0
2660 Wasserman	628.3	E	137	9.2
2780 Monnig	681.8	E	91	4.8
2795 Lepage	40.368	E	107	6.1
2819 Ensor	161.66	E	130	9.7
2837 Griboedov	3.94988	C	119	12.3
2909 Hoshi-no-ie	311.3	CE	188	21.3
2949 Kaverznev	83.81	CE	77	7.0
2967 Vladisvyat	8.3739	E	176	32.9
3158 Anga	10.3203	E	113	7.3
3181 Ahnert	1187.1	E	134	8.0
3214 Makarenko	249.2	E	165	21.2
3311 Podobed	191.43	E	127	17.3
3346 Gerla	26.239	E	208	34.6
3365 Recogne	254.2	E	114	17.7
3380 Awaji	87.74	E	125	–
3650 Kunming	12.3703	E	111	26.6
3681 Boyan	966.3	C	107	4.2
3702 Trubetskaya	8.2905	E	207	18.2
3863 Gilyarovskij	12.9588	E	114	6.5
3955 Bruckner	7.5492	E	205	18.1
4101 Ruikou	3.13391	E	76	8.2
4103 Chahine	105.08	CE	208	13.3
4121 Carlin	97.78	E	74	6.9
4129 Richelen	288.8	E	75	5.4
4256 Kagamigawa	1014.7	E	110	7.5
4292 Aoba	291.1	C	97	24.7
4380 Geyer	7.7282	E	120	16.9
4593 Reipurth	5.9985	E	96	12.3
5042 Colpa	169.62	E	151	20.2
5077 Favaloro	4.59045	E	68	4.5
5203 Pavarotti	6.93199	E	97	5.0
5238 Naozane	80.61	E	69	5.9
5650 Mochihito-o	601.3	CE	196	11.4
5886 Rutger	3.32503	E	142	17.3
6064 Holasovice	337.7	C	71	3.8
6917 –	351.9	CE	74	4.4

**Table A.4.** continued.

Asteroid	<i>P</i> [hours]	M	<i>N<sub>A</sub></i>	<i>D</i> [km]
7387 Malbil	7.5498	E	64	–
10314 –	1311.5	E	73	21.8
10426 Charlierouse	36.975	E	147	9.2
11358 –	10.7927	E	84	13.6
11923 –	7.1288	E	62	2.8
13249 Marcallen	190.9	E	123	20.8
13832 –	98.43	E	169	37.5
14720 –	108.14	E	149	8.5
20602 –	7.3061	E	79	23.7
27396 Shuji	203.68	E	106	23.9

**Notes.** We provide the sidereal rotational period *P* (its uncertainty is on the order of the last digit). The method column (M) indicates whether the rotation period was derived by the convex inversion approach (C), the ellipsoid approach (E), or both (CE). The final two columns are the number of ASAS-SN measurements *N<sub>A</sub>* and the size *D* from the MP3C database.